



## RESEARCH ARTICLE

10.1029/2021JD035657

### Special Section:

Fire in the Earth System

### Key Points:

- Ash-bearing particles with diameters smaller than several microns can be one of the major aerosol components in biomass burning (BB) smoke
- Fine ash-bearing particles can act as cloud condensation or ice nuclei and influence cloud properties
- The global emission of fine ash aerosol mass from BB is estimated to be  $\sim 11.6 \text{ Tg yr}^{-1}$

### Supporting Information:

Supporting Information may be found in the online version of this article.

### Correspondence to:

K. Adachi,  
[adachik@mri-jma.go.jp](mailto:adachik@mri-jma.go.jp)

### Citation:

Adachi, K., Dibb, J. E., Scheuer, E., Katich, J. M., Schwarz, J. P., Perring, A. E., et al. (2022). Fine ash-bearing particles as a major aerosol component in biomass burning smoke. *Journal of Geophysical Research: Atmospheres*, 127, e2021JD035657. <https://doi.org/10.1029/2021JD035657>

Received 3 AUG 2021

Accepted 24 DEC 2021

### Author Contributions:

**Conceptualization:** Kouji Adachi, James Crawford, Robert J. Yokelson, Peter R. Buseck














**Funding acquisition:** Kouji Adachi, Peter R. Buseck

**Investigation:** Kouji Adachi, Jack E. Dibb, Eric Scheuer, Joseph M. Katich, Joshua P. Schwarz, Anne E. Perring, Braden Mediavilla, Hongyu Guo, Pedro Campuzano-Jost, Jose L. Jimenez, Amber J. Soja, Naga Oshima, Mizuo Kajino, Takeshi Kinase, Lawrence Kleinman, Arthur J. Sedlacek

© 2022 The Authors.

This is an open access article under the terms of the [Creative Commons Attribution-NonCommercial License](https://creativecommons.org/licenses/by-nc/4.0/), which permits use, distribution and reproduction in any medium, provided the original work is properly cited and is not used for commercial purposes.

## Fine Ash-Bearing Particles as a Major Aerosol Component in Biomass Burning Smoke

Kouji Adachi<sup>1</sup> , Jack E. Dibb<sup>2</sup> , Eric Scheuer<sup>2</sup>, Joseph M. Katich<sup>3,4</sup> , Joshua P. Schwarz<sup>3</sup> , Anne E. Perring<sup>4,5</sup>, Braden Mediavilla<sup>5</sup>, Hongyu Guo<sup>4,6</sup> , Pedro Campuzano-Jost<sup>4,6</sup> , Jose L. Jimenez<sup>4,6</sup> , James Crawford<sup>7</sup> , Amber J. Soja<sup>7,8</sup> , Naga Oshima<sup>1</sup> , Mizuo Kajino<sup>1</sup> , Takeshi Kinase<sup>1,9</sup>, Lawrence Kleinman<sup>10</sup>, Arthur J. Sedlacek III<sup>10</sup> , Robert J. Yokelson<sup>11</sup> , and Peter R. Buseck<sup>12</sup>

<sup>1</sup>Department of Atmosphere, Ocean and Earth System Modelling Research, Meteorological Research Institute, Tsukuba, Japan, <sup>2</sup>Institute for the Study of Earth, Oceans, and Space, University of New Hampshire, Durham, NH, USA, <sup>3</sup>Chemical Sciences Laboratory, National Oceanic and Atmospheric Administration, Boulder, CO, USA, <sup>4</sup>Cooperative Institute for Research in Environmental Sciences, University of Colorado Boulder, Boulder, CO, USA, <sup>5</sup>Department of Chemistry, Colgate University, Hamilton, NY, USA, <sup>6</sup>Department of Chemistry, University of Colorado Boulder, Boulder, CO, USA, <sup>7</sup>NASA Langley Research Center, Hampton, VA, USA, <sup>8</sup>National Institute of Aerospace, Hampton, VA, USA, <sup>9</sup>Now at Institute of Arctic Climate and Environmental Research, Japan Agency for Marine-Earth Science and Technology, Yokohama, Japan, <sup>10</sup>Environmental and Climate Sciences Department, Brookhaven National Laboratory, Upton, NY, USA, <sup>11</sup>Department of Chemistry and Biochemistry, University of Montana, Missoula, MT, USA, <sup>12</sup>School of Earth and Space Exploration & School of Molecular Sciences, Arizona State University, Tempe, AZ, USA

**Abstract** Biomass burning (BB) events are occurring globally with increasing frequency, and their emissions are having more impacts on human health and climate. Large ash particles are recognized as a BB product with major influences on soil and water environments. However, fine-ash particles, which have diameters smaller than several microns and characteristic morphologies and compositions (mainly Ca and Mg carbonates), have not yet been explicitly considered as a major BB aerosol component either in field observations or climate models. This study measured BB aerosol samples using transmission electron microscopy (TEM) and ion chromatography during the Fire Influence on Regional to Global Environments and Air Quality (FIREX-AQ) campaign. We show that significant amounts of fine ash-bearing particles are transported >100 km from their fire sources. Our environmental chamber experiments suggest that they can act as cloud condensation and ice nuclei. We also found considerable amounts of fine ash-bearing particles in the TEM samples collected during previous campaigns (Biomass Burning Observation Project and Megacity Initiative: Local and Global Research Observations). These ash particles are commonly mixed with organic matter and make up  $\sim 8\%$  and  $5\%$  of BB smoke by number and mass, respectively, in samples collected during the FIREX-AQ campaign. The measured ash-mass concentrations are approximately five times and six times greater than those of BB black carbon and potassium, respectively, scaling to an estimated global emission of  $11.6 \text{ Tg yr}^{-1}$  with a range of  $8.8\text{--}16.3 \text{ Tg yr}^{-1}$ . Better characterization and constraints on these fine ash-bearing particles will improve BB aerosol measurements and strengthen assessments of BB impacts on human health and climate.

**Plain Language Summary** Biomass burning (BB) events occur globally and impact climate and human health. Ash particles larger than  $\sim 10 \mu\text{m}$  are well known as the main products of BB that contaminate the soil and water near the source regions. On the other hand, ash particles having diameters smaller than several microns, which are inhalable and can be transported long distances, are not yet recognized as a major aerosol component of BB smoke. This study reveals that such fine ash-bearing particles are abundant in number ( $\sim 8\%$ ) and mass ( $\sim 5\%$ ) within BB smoke. The global emission of fine ash particles is estimated to be  $11.6 \text{ Tg yr}^{-1}$  with a range of  $8.8\text{--}16.3 \text{ Tg yr}^{-1}$ . By considering their abundance and properties, we will strengthen assessments of BB impacts on human health and climate.

## 1. Introduction

Biomass burning (BB) occurs globally and significantly impacts climate, regional air quality, ecosystems, and human health (Andreae et al., 2004; Crutzen & Andreae, 1990; Hirsch & Koren, 2021; McClure & Jaffe, 2018; Reisen et al., 2015; Schill et al., 2020). In 2019 and 2020, severe BB events damaged ecosystems, buildings, and

**Methodology:** Kouji Adachi, Jack E. Dibb

**Project Administration:** Jack E. Dibb, Joshua P. Schwarz, James Crawford, Lawrence Kleinman, Arthur J. Sedlacek, Robert J. Yokelson, Peter R. Buseck

**Writing – original draft:** Kouji Adachi, Peter R. Buseck

**Writing – review & editing:** Kouji Adachi, Jack E. Dibb, Joseph M. Katich, Joshua P. Schwarz, Anne E. Perrin, Hongyu Guo, Pedro Campuzano-Jost, Jose L. Jimenez, James Crawford, Amber J. Soja, Naga Oshima, Mizuo Kajino, Lawrence Kleinman, Arthur J. Sedlacek, Robert J. Yokelson

air quality in the Amazon basin, Australia, and the United States (Hirsch & Koren, 2021; Kganyago & Shikwambana, 2020). Particulate BB emissions have been detected across the globe, including North America (Hecobian et al., 2011; Hudson et al., 2004), the remote troposphere (Brocchi et al., 2018; Hodzic et al., 2020; Schill et al., 2020), and the Arctic (Adachi et al., 2021; Brock et al., 2011). BB events have been an important factor influencing global climate since before the industrial revolution. BB emissions are also known to cause health problems such as respiratory morbidity (Pardo et al., 2020; C. E. Reid et al., 2016). Their frequency and severity are predicted to increase in the future due to increasing drought and temperatures caused by human-induced climate change (Abatzoglou & Williams, 2016; Dennison et al., 2014), although some areas in the western US suffer from a deficit of naturally occurring fire due to historic management practices that emphasized fire suppression (Parks et al., 2015). These studies suggest that human activities significantly disturb the natural role of fire.

One of the impacts of BB is that vast amounts of ash are produced. Ash particles larger than  $\sim 10 \mu\text{m}$  (“biomass bottom ash”) are mostly deposited on soil, trees, or buildings near the BB source due to their rapid gravitational settling, and some are washed out into runoff (Bodí et al., 2014; Radke et al., 1991). Fly ash particles are also emitted from coal combustion (Umo et al., 2015). In addition to these large biomass bottom ash and fly ash, we find that large amounts of fine ash particles with diameters smaller than several micrometers are present aloft in aerosol samples at distances over 100 km from the BB sources during BB-focused campaigns in the USA and Mexico (Figure 1). Different from large ash particles, the fine ash-bearing particles are suspended in the air for several days or more and behave as aerosols. They occurred either by themselves, with coatings of organic matter, or with attachments of soot, tarballs, or other substances, and we call them ash-bearing particles. These ash-bearing particles were measured from aerosol particles collected on transmission electron microscopy (TEM) grids and were defined as those containing both Ca and Mg ( $>0.5$  weight %). Due to their inhalable size range and abundant emissions, they likely exert previously unrecognized impacts on climate, regional air quality, and human health. However, even fundamental information such as the occurrence, abundance, and emission inventories of BB fine ash-bearing particles has not been explicitly reported as an aerosol component from BB due to unawareness of these particles and a lack of direct detection techniques. This information is important for improving our knowledge about BB climate effects and impacts on human health.

Some studies using electron microscopy have shown similar Ca- and Mg-bearing particles in coarse ( $\text{PM}_{10-2.5}$  and  $\text{PM}_{10}$ ) BB particles (Sparks & Wagner, 2021; Wagner et al., 2012). Others have reported Ca- and Mg-containing aerosol particles in BB samples, similar to the fine ash-bearing particles in the current study, but without identifying their origin (Li et al., 2003; Yokelson et al., 2011). These studies suggested that fine ash-bearing particles are emitted from widely varying types of BB.

We analyzed aerosol particles emitted from BB, both wildfires and agricultural burning, during the Fire Influence on Regional to Global Environments and Air Quality (FIREX-AQ) campaign using TEM and ion chromatography (IC), which measure nonvolatile materials and soluble fractions of aerosol particles, respectively. We also measured TEM samples collected in BB smoke plumes during the Biomass Burning Observation Project (BBOP; Sedlacek et al., 2018) and the Megacity Initiative: Local and Global Research Observations (MILAGRO; Molina et al., 2010) campaigns to confirm the ash particle occurrences at different locations and sampling periods. Using compositional markers, we identified fine ash-bearing particles at an individual particle scale and measured the bulk mass of fine ash components, allowing the first quantitative assessments of their occurrences and abundances in BB smoke.

## 2. Materials and Methods

### 2.1. Biomass Burning Field Campaigns and TEM Samplings

All TEM smoke samples were directly collected within smoke plumes from wildfires, agricultural fires, and other fires during research flights for the FIREX-AQ, BBOP, and MILAGRO campaigns. More than 500 TEM samples were collected over the western and southeastern United States during the FIREX-AQ campaign in the summer of 2019 (<https://csl.noaa.gov/projects/firex-aq/>). The sampling was conducted using the NASA DC-8 aircraft ([https://airbornescience.nasa.gov/aircraft/DC-8\\_-\\_AFRC](https://airbornescience.nasa.gov/aircraft/DC-8_-_AFRC)). During each flight, we collected smoke and background (nonsmoke) samples of aerosol particles using an impactor sampler (AS-24W, Arios Inc., Tokyo, Japan), with two TEM grids containing overlapping lacey carbon (top; U1001, EM-Japan, Tokyo, Japan) and Formvar substrates (bottom; U1007, EM-Japan, Tokyo, Japan). This study mainly used the Formvar substrate.

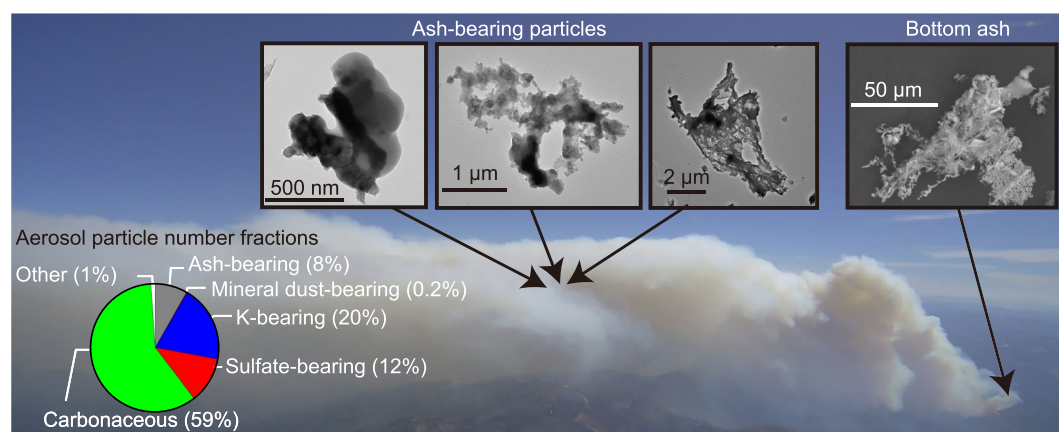


**Figure 1.** Schematic of the emission of ash-bearing particles and their number fractions. The wildfire picture was taken from the Shady fire on July 25, 2019, with the forward camera onboard the NASA DC-8 during the FIREX-AQ campaign. The smoke top was  $\sim 5$  km above mean sea level. In the pie chart, the aerosol particle number fractions are average values for the FIREX-AQ BB samples measured using TEM. Images of ash-bearing particles were taken from the samples collected on July 25 (left) and August 23 (center and right). The biomass bottom ash particle was obtained from a pine ash sample. See Figures S1–S3, S6, and S7 in Supporting Information S1 for a comprehensive data set of the images and number fractions.

The small and large 50% cutoff sizes were aerodynamic diameters of 100 and 700 nm, respectively. Sampling was conducted to cover each transect of BB smoke, with sampling times of  $\sim 1$ –3 min and an airflow rate of 1.0 L/min. We chose nine research flights measuring relatively intense BB events and analyzed 221 TEM grids (53,727 particles in total) using scanning TEM equipped with an energy-dispersive X-ray spectrometer (STEM-EDS; Table 1; Figure S1 in Supporting Information S1).

We analyzed BB samples collected during the BBOP campaign (Sedlacek et al., 2018) in the summer of 2013 in the northwestern United States and the MILAGRO campaign (Molina et al., 2010) in the spring of 2006 in Mexico. During the BBOP campaign, we analyzed 52 TEM samples with 10,772 particles from four research flights conducted on a Gulfstream-1 (G-1) aircraft (Table 2). An impactor sampler (AS-16W, Arios Inc., Tokyo, Japan) with a lacey carbon substrate (Ted Pella, CA, USA, Type 01,881) was used. The sampling details are described in Adachi et al. (2018, 2019). In the current study, we reanalyzed the EDS data reported in Adachi et al. (2019) to classify ash particles. For the MILAGRO campaign samples, we analyzed 2,608 particles from 10 BB samples taken during four research flights conducted on the US Forest Service Twin Otter aircraft (Table 3). A 3-stage impactor sampler (MPS-3, California Measurements, Inc., California, USA) was used for the sampling (Adachi & Buseck, 2008). Further details of the MILAGRO samples are provided in Adachi and Buseck (2008) and Yokelson et al. (2009, 2011).

## 2.2. TEM Measurements

A transmission electron microscope (JEM-1400, JEOL, Tokyo, Japan) equipped with an EDS (X-Max 80, Oxford Instruments, Tokyo, Japan) was used in TEM and STEM modes. An acceleration voltage of 120 keV and an acquisition time of 20 s were used for STEM-EDS measurements. We first took  $\sim 30$  TEM images across the sample grid and then chose two or more representative areas with  $\sim 100$  particles at a magnification of  $\times 6,000$  in STEM mode. Particles and substrates have different compositions and thicknesses, resulting in different brightness within STEM images. Thus, aerosol particles were identified from binary STEM images using appropriate thresholds that distinguish particles from the substrate (Adachi et al., 2019). Particle shapes from the binary image, including area-equivalent diameters and shape factor, and EDS spectra were obtained from the selected particles. The area-equivalent diameter tends to be approximately two times larger than the volume equivalent diameter because particles are spread over substrates (Zhang et al., 2020), and volatile and semi-volatile aerosol particles such as volatile organic compounds and nitrates would be lost after the sampling and in the vacuum TEM chamber. The smallest particle cutoff sizes for STEM-EDS analyses were area-equivalent diameters of 0.25  $\mu\text{m}$  for FIREX-AQ and MILAGRO samples and 0.05  $\mu\text{m}$  for BBOP samples in the STEM images (pixel number  $> 100$  for each particle image at the measured magnifications). Relative weight percentages within each particle measured by

**Table 1**  
Information on the FIREX-AQ 2019 TEM Samples

Date	Main fires	State	Latitude	Longitude	TEM sample #	Particle #	Primary fuels <sup>a</sup>
25-July	Shady	ID	44.52	115.02	22	6,130	Modified or Managed Mesic Timber Litter; Modified or Managed Xeric Grass Shrub
6-August	Horsefly	MT	46.96	112.44	24	6,317	Subalpine fir-lodgepole pine-whitebark pine-Engelmann spruce forest; Douglas-fir-Pacific ponderosa pine/oceanspray forest
7-August	Williams Flats	WA	47.94	118.62	24	5,873	Douglas-fir-Pacific ponderosa pine/oceanspray forest; Idaho fescue-bluebunch wheatgrass grassland
8-August	Williams Flats	WA	47.94	118.62	21	5,430	Douglas-fir-Pacific ponderosa pine/oceanspray forest; Idaho fescue-bluebunch wheatgrass grassland
12-August	Castle	AZ	36.53	112.23	24	6,062	Ponderosa pine-two-needle pinyon-Utah juniper forest; Douglas-fir-white fir-ponderosa pine forest
13-August	Castle	AZ	36.53	112.23	24	5,660	Ponderosa pine-two-needle pinyon-Utah juniper forest; Douglas-fir-white fir-ponderosa pine forest
15-August	Sheridan	AZ	34.68	112.89	22	5,139	Pinyon-Utah juniper forest; Turbinella oak-alderleaf mountain mahogany shrubland
16-August	Sheridan	AZ	34.68	112.89	24	5,801	Pinyon-Utah juniper forest; Turbinella oak-alderleaf mountain mahogany shrubland
3-September	Agricultural BB	IL, MO, AR, MS <sup>b</sup>	33.5–37.5	88.6–91.7	36	7,315	Crop residue (rice and corn)
Total					221	53,727	

<sup>a</sup>Fuel characteristic classification system (FCCS) name except the agricultural BB (3-September). <sup>b</sup>Agricultural samples were collected from various occurrences of smoke in the region.

STEM-EDS were obtained for C, N, O, Na, Mg, Al, Si, P, S, Cl, K, Ca, Ti, Mn, Fe, and Zn. The detection limits were obtained from one sigma of the measured peak intensities and were generally 0.02 weight %. The EDS technique has relatively large uncertainties for light elements, and the uncertainty of the EDS quantification values was within ~5 weight % for C, N, O, and S (Adachi et al., 2019). To directly compare the TEM results with aerosol mass fractions measured using IC and the aerosol mass spectrometer (AMS), the mass fractions in samples measured using TEM were estimated from the sum of all particle mass fractions obtained from the weight % and their particle volumes, which were calculated from their area-equivalent diameters by assuming that they were spherical. Although TEM measurements only analyze a limited fraction of collected particles, the TEM results are generally consistent with those of bulk measurements by IC and AMS, supporting the representativeness of the TEM samples used in this study. The limitations of the comparison of the TEM results with the IC and AMS measurements are discussed in Text S1 in Supporting Information S1.

### 2.3. Particle Classifications

Measured aerosol particles were classified into six particle types based on their compositions (Figure 2): ash-bearing particles (Mg, Ca > 0.5 weight %), mineral dust (soil)-bearing particles (Al, Fe > 0.5 weight %), K-bearing particles (K > 2 weight %), sulfate-bearing particles (S > 2 weight %), carbonaceous particles without major inclusions (C + O > 90 weight %), and others (none of above). Many particles were mixtures of two or more particle types and were classified into a single category based on the flow chart. For example, when ash particles were embedded within organic matter, they were classified into the ash-bearing particle category. Thus, the number fractions are likely underestimated for secondary aerosol particles such as organic matter (carbonaceous) and

**Table 2**  
Information on the BBOP 2013 TEM Samples

Date	Main fires	State	Latitude	Longitude	TEM sample #	Particle #	Primary fuels <sup>a</sup>
26-July	Mile Marker 28	WA	46.0–46.3	119.5–120.6	12	2,485	Grasslands, shrub brush, timber, and litter
30-July A	Colockum Tarps	WA	46.7–47.3	119.3–120.4	14	3,389	Grass, timber, and litter
30-July B	Colockum Tarps	WA	47.1–47.3	119.8–120.5	15	2,336	Grass, timber, and litter
21-August	Government Flats	OR	45.5–46.1	119.6–121.8	11	2,297	Timber, hardwoods, pine, and fir
Total					52	10,507	

<sup>a</sup>Kleinman et al. (2020).

sulfates, both of which are commonly mixed with other particle types. We chose a relatively small weight % (0.5 weight %) for the threshold value of Mg, Ca, Al, and Fe to detect ash-bearing and mineral dust-bearing particles as they are important but relatively minor components within each particle. K-bearing particles are mostly mixtures of KCl and K<sub>2</sub>SO<sub>4</sub>, which are important tracers of BB smoke.

## 2.4. Other Instruments Employed During the FIREX-AQ Campaign

### 2.4.1. Ion Chromatography (IC)

The soluble acidic gases and aerosols analysis system using IC was used to measure aqueous extracts of the bulk aerosol particles collected on Teflon filters during DC-8 flights. The details are described elsewhere (Heim et al., 2020; Scheuer et al., 2003). Aerosol particles were sampled isokinetically through a forward-facing aerosol inlet onto a filter. The 50% upper cutoff size of the inlet was estimated to be ~4.1 μm in aerodynamic diameter at an airspeed of 120 m/s (McNaughton et al., 2007). Ions were extracted from the filter into deionized water, and the IC was used to quantify soluble ions (Cl<sup>-</sup>, Br<sup>-</sup>, NO<sub>3</sub><sup>-</sup>, SO<sub>4</sub><sup>2-</sup>, C<sub>2</sub>O<sub>4</sub><sup>2-</sup>, Na<sup>+</sup>, NH<sub>4</sub><sup>+</sup>, K<sup>+</sup>, Ca<sup>2+</sup>, and Mg<sup>2+</sup>) in the sampled air (μg m<sup>-3</sup> at STP). The cation channel of the IC uses an acidic eluent (methanesulfonic acid), and thus particles that are soluble in weak acids, such as CaCO<sub>3</sub>, can be measured. See more discussion of solubility in Text S2 in Supporting Information S1. The IC will lose some fraction of highly volatile materials such as ammonium nitrate (Heim et al., 2020). Sampling times ranged from 2 to 15 min depending on the smoke transect. Mixing ratios were corrected using blank filters.

### 2.4.2. Aerosol Mass Spectrometer (AMS)

Submicron aerosol mass concentrations were measured online at 1–5 Hz using an Aerodyne high-resolution time-of-flight aerosol mass spectrometer, which detects the non-refractory aerosol components by impaction on a vaporizer at 600°C, followed by electron ionization and time-of-flight mass spectral analysis (Canagaratna et al., 2007; DeCarlo et al., 2006; Nault et al., 2018). As operated in FIREX-AQ, the AMS inlet had a 50% cutoff size of 960 nm in vacuum aerodynamic diameter, equivalent to approximately 870 nm in aerodynamic diameter for typical FIREX-AQ plumes. The AMS measures aerosol particle compositions in near real time (0.3 s inlet residence time), resulting in minimal losses of volatile materials. The sum of organic aerosol, sulfate, nitrate, ammonium, and chloride was used to determine PM<sub>1</sub>.

**Table 3**  
Information on the MILAGRO 2006 TEM Samples

Date	Primary fuels	TEM sample #	Particle #	Reference
20-March	Crop residue/deforestation	2	618	Yokelson et al. (2011)
22-March	Crop residue/deforestation	2	495	Yokelson et al. (2009)
25-March	Pine-Oak Rural	2	483	Yokelson et al. (2011)
27-March	Savanna	2	529	Yokelson et al. (2011)
28-March	Pine-Oak Rural	2	483	Yokelson et al. (2011)
Total		10	2,608	

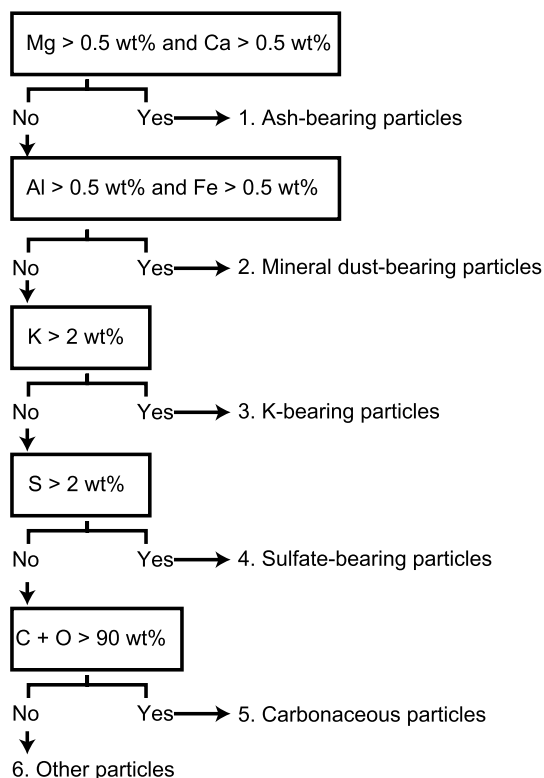


**Figure 2.** Flow chart for classifying individual particles into six categories based on STEM-EDS measurements.

### 2.4.3. Single Particle Soot Photometer (SP2)

Refractory black carbon (BC) mass concentrations in the particle size range 90–550 nm were measured using an SP2 (Droplet Measurement Technology, Inc, Longmont, CO, USA), a laser-induced incandescence instrument. These concentrations were scaled upwards by 8% for wildfires and by 15% for agricultural burning to account for BC mass outside of instrumental detection limits, assuming a single log-normal mode in the accumulation mode. The details of the SP2 are described in Schwarz et al. (2008).

### 2.5. Optical Microscope With Environmental Chamber Measurements

An optical microscope (Axio Imager M2m; Carl Zeiss, Tokyo, Japan) with an environmental chamber with a volume of  $\sim 50$  cm<sup>3</sup> (Rh10002L; Japan High Tech Co., Ltd., Fukuoka, Japan) was used to capture optical microscopic images of TEM grid samples with a controlled temperature and RH within the environmental chamber. In the chamber, we can control the sample temperature using a liquid nitrogen/heater and chamber RH by introducing water vapor and dry air. The samples were mounted on a heater block, which controlled the sample temperature. The RH around the sample was controlled and monitored in the environmental chamber at room temperature. The sample RH was calculated from the sample temperature and the chamber RH. We used six coarse-mode BB samples ( $>700$  nm in aerodynamic diameter) collected on July 24 at 23:21, August 17 at 02:02, August 17 at 02:08, August 17 at 02:18, August 17 at 02:22, and August 17 at 02:33 (UTC) during the FIREX-AQ campaign for both cloud condensation nuclei (CCN) and ice-nucleating particle (INP) measurements. Increases and decreases in RH values and temperatures for the CCN and INP experiments, respectively, were repeated several times for each sample.

During the CCN experiments, RH was increased to  $\sim 100\%$  at the chamber temperatures ranging from 10°C to 21°C. A CCD camera on the optical microscope recorded shape changes. Standard samples (KCl, NaCl, Na<sub>2</sub>SO<sub>4</sub>,

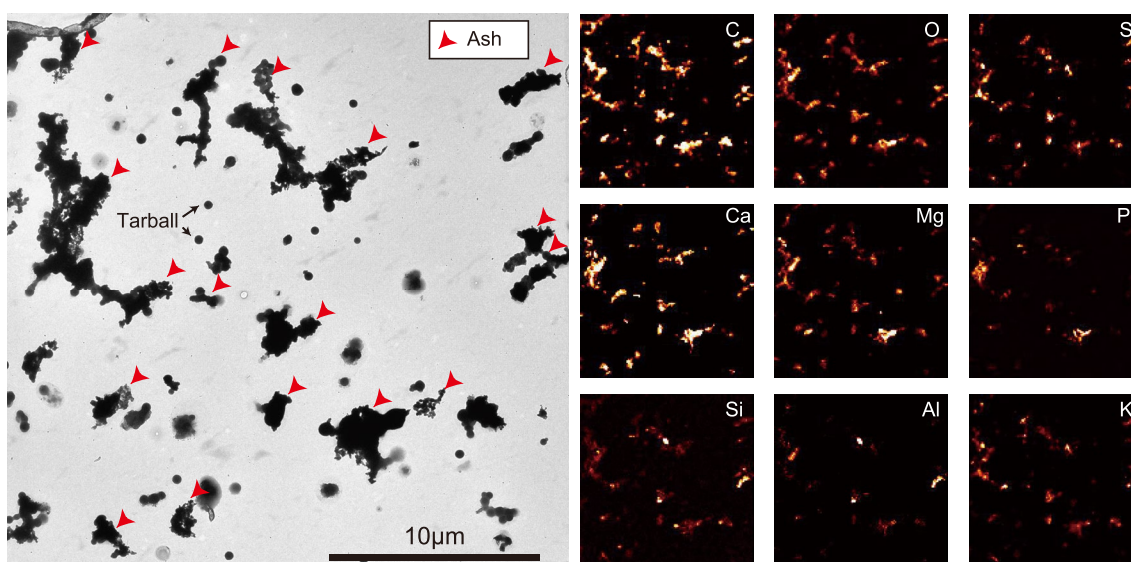


**Figure 3.** Example of a TEM image and elemental mappings of C, O, S, Ca, Mg, P, Si, Al, and K. The sample was collected from the Sheridan fire (August 17, 2019, 02:18 UTC) during the FIREX-AQ campaign. The ash-bearing particle number fraction of this sample is relatively high (42%). Ash components mainly consist of Ca, Mg, P, C, and O. Organic materials mainly contain C and O. Particles generally consist of several components, including ash and organic materials.

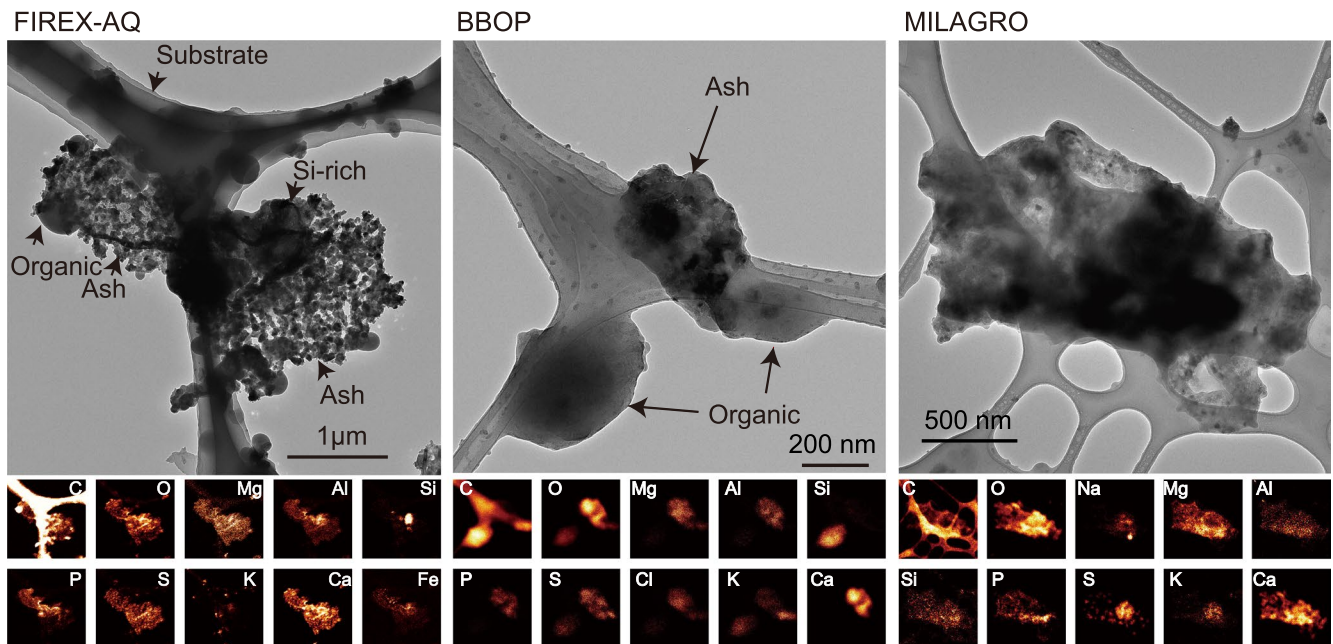


**Figure 4.** TEM image and elemental distributions of ash-bearing particles. Left: An ash-bearing particle collected on a lacey-carbon substrate from the FIREX-AQ campaign on July 25 at 22:47. The C mapping image has enhanced contrast to show C in the ash-bearing particle, which has less C than the substrate and organic matter. Middle: An ash-bearing particle collected during the BBOP campaign on August 21, 2013. Right: An ash-bearing particle collected during the MILAGRO campaign on March 27, 2006.

and  $(\text{NH}_4)_2\text{SO}_4$  were used to check the RH by comparing their theoretical and measured deliquescence RH values, confirming that the measured RH values agreed with the theoretical values to within  $\pm 1\%$ .

During the INP measurements, the maximum error range of the measured temperature was  $\pm 3^\circ\text{C}$  at  $-38^\circ\text{C}$ . RH values in the chamber were kept at  $\sim 4\% - 8\%$  at the chamber temperature. From the stage temperature and the

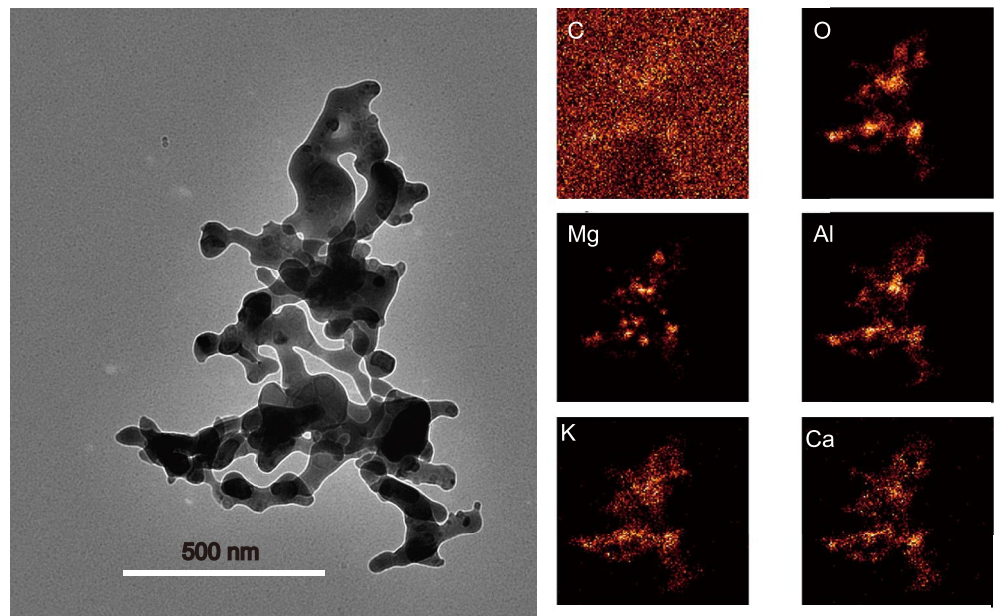


**Figure 5.** Example of a TEM image and elemental distributions for a laboratory-generated pine ash particle. A piece of pine branch was heated in a furnace at  $500^\circ\text{C}$  with air, turning it completely into ash. The biomass bottom ash particles were placed on a TEM grid.

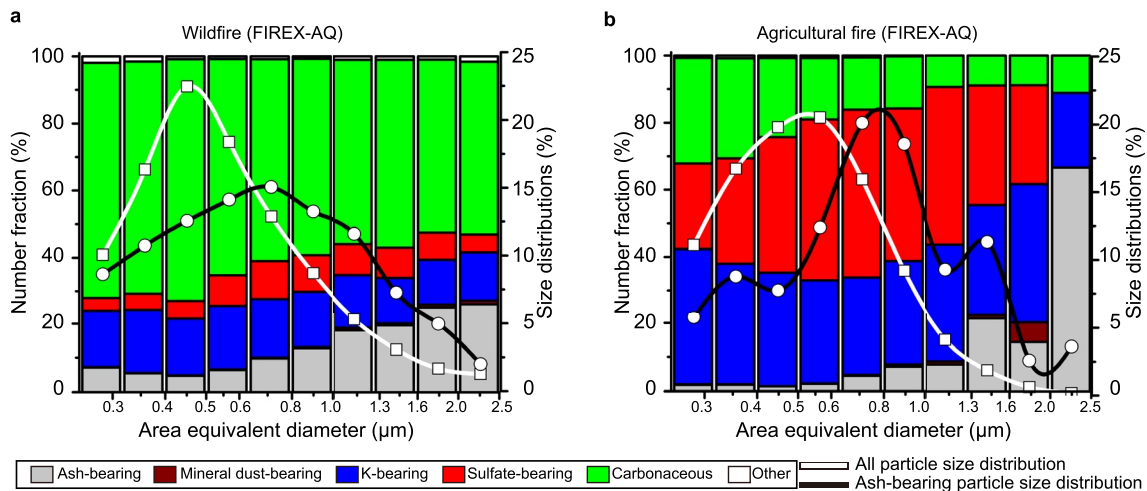


**Figure 6.** Size-dependent number fractions of aerosol particles from the FIREX-AQ campaign: (a) wildfire and (b) agricultural fire samples (left scales). Right scales: normalized size distributions of all particles (white lines) and ash-bearing particles (black lines). See Figure S8 in Supporting Information S1 for all flight data.

chamber RH value, the RH value near the stage was estimated to be  $\sim 300\%$  after cooling. However, the actual RH value around the particles will be smaller than the estimated value because water vapor is consumed by particles that absorb water or develop ice crystals. When a particle grows an ice crystal, other particles near the INP cannot form ice due to the limited availability of water. A cooling rate of  $30^\circ\text{C}/\text{minute}$  was used.

### 2.6. Emission Inventories of Black Carbon and Potassium From Biomass Burning

The annual and daily BB emissions for climate models in 2019 varied depending on emission estimates. Thus, we chose multiple estimates that are commonly used in climate models (Table S1 in Supporting Information S1). They were obtained from the Global Fire Assimilation System (GFAS) data set (Kaiser et al., 2012), the Global Fire Emissions Database (GFED v4.1; van der Werf et al., 2017), and the BB emission inventory for use in the Coupled Model Intercomparison Project Phase 6 (CMIP6; Eyring et al., 2016; Gidden et al., 2019). GFAS calculates BB emissions by assimilating fire radiative power observations from the MODIS instruments onboard the Terra and Aqua satellites (Kaiser et al., 2012). GFED provides fire emissions based on burned areas and hotspot

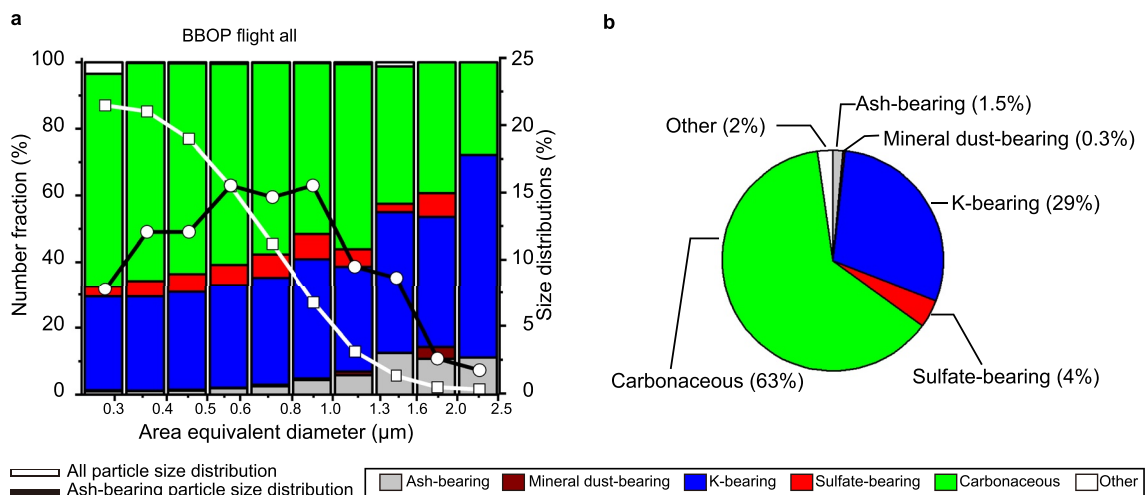


**Figure 7.** Number fractions of aerosol particles collected during the BBOP campaign. (a) Size-dependent number fractions (left scales). Right scale: normalized size distributions of all particles (white lines) and ash-bearing particles (black lines). (b) The averaged number fractions. The measured particle number is 12,406. The size bins are  $<0.32$ ,  $0.32\text{--}0.40$ ,  $0.40\text{--}0.50$ ,  $0.50\text{--}0.63$ ,  $0.63\text{--}0.79$ ,  $0.79\text{--}1.00$ ,  $1.00\text{--}1.26$ ,  $1.26\text{--}1.58$ ,  $1.58\text{--}2.00$ , and  $>2.00$   $\mu\text{m}$ . See Figure S9 in Supporting Information S1 for all flight data.



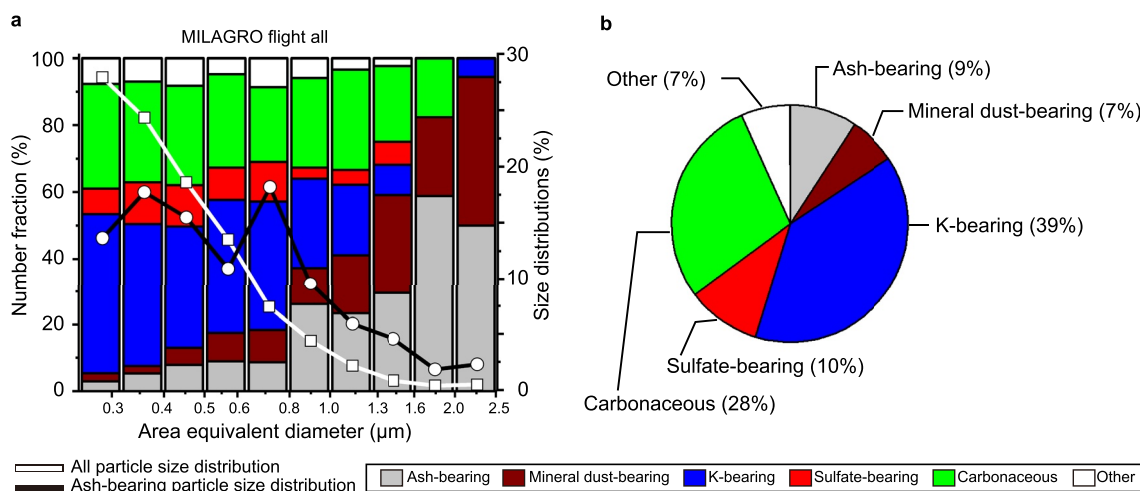


**Figure 8.** Number fractions of aerosol particles collected during the MILAGRO campaign. (a) Size-dependent number fractions (left scales). Right scale: normalized size distributions of all particles (white lines) and ash-bearing particles (black lines). (b) The averaged number fractions. Although the fractions of K-bearing particles were higher than those of carbonaceous particles, K-bearing particles were mostly mixed with organic materials (e.g., Figure S5 in Supporting Information S1), which are likely dominant in mass fractions. The particle number is 2,608. The size bins are  $<0.32$ ,  $0.32\text{--}0.40$ ,  $0.40\text{--}0.50$ ,  $0.50\text{--}0.63$ ,  $0.63\text{--}0.79$ ,  $0.79\text{--}1.00$ ,  $1.00\text{--}1.26$ ,  $1.26\text{--}1.58$ ,  $1.58\text{--}2.00$ , and  $>2.00$   $\mu\text{m}$ .

detection. In the BB emission estimates of Andreae (2019), we used the sum of savanna and grassland, tropical forest, temperate forest, boreal forest, and agricultural residue emissions (total emissions except for biofuel, peat, and charcoal burning) for determinations of BC and K.

### 3. Results and Discussion

#### 3.1. Occurrences of Fine Ash-Bearing Particles

During the FIREX-AQ campaign conducted in the USA in 2019, significant numbers of ash-bearing particles were found in TEM aerosol samples with aerodynamic diameters of  $100\text{--}700$  nm in 50% cutoff sizes or area-equivalent diameters of  $\sim 250\text{--}4,000$  nm in TEM images (Figures 3, 4, and S2–S3 in Supporting Information S1). Similar ash-bearing particles were found in samples from the BBOP and MILAGRO campaigns, which were conducted in different years and at different locations (Figures 4 and S4–S5 in Supporting Information S1). Except for their small sizes, the composition and shapes of these particles were similar to biomass bottom ash particles observed in ambient samples (J. S. Reid & Hobbs, 1998), laboratory-generated samples (Jöller et al., 2005; Kleinhans et al., 2018; Vassilev et al., 2010, 2012, 2013), and pine ash particles generated in our laboratory (Figures 5 and S6 in Supporting Information S1). TEM images show that ash-bearing particles from ambient BB smoke commonly have aggregated shapes with complicated compositions, predominantly calcium with other elements (e.g., C, O, Mg, Al, Si, P, S, and Fe in Figures 3 and 4). They also have coatings or attachments of organic matter, potassium salts, and other components.

When observing individual aerosol particles in BB smoke using TEM, the nonvolatile particles mainly consist of carbonaceous materials, which commonly embed other materials such as ash, potassium salts, sulfate, and mineral dust (Figures 3 and 4). Thus, we classified aerosol particles by focusing on these inclusions and measured their number fractions by STEM-EDS. These particles also included carbonaceous aerosol particles without major inclusions (59%; this and subsequent values are the average number fractions of all BB samples collected during FIREX-AQ), K-bearing particles (e.g., KCl and  $\text{K}_2\text{SO}_4$ ) (20%), sulfate-bearing particles (12%), ash-bearing particles (8%), and mineral dust-bearing particles characterized by Fe and Al (0.2%; Figures 1 and S7 in Supporting Information S1). The number fractions varied depending on particle size, and larger particle bins had larger ash-bearing particle fractions in samples from the three campaigns (Figures 6–8 and S8–S9 in Supporting Information S1).

The number fractions of ash-bearing particles among all TEM-measured particles varied depending on the fire emitting the smoke (0.8%–25%; Figures 9 and S7 in Supporting Information S1). The fuel type, combustion temperature

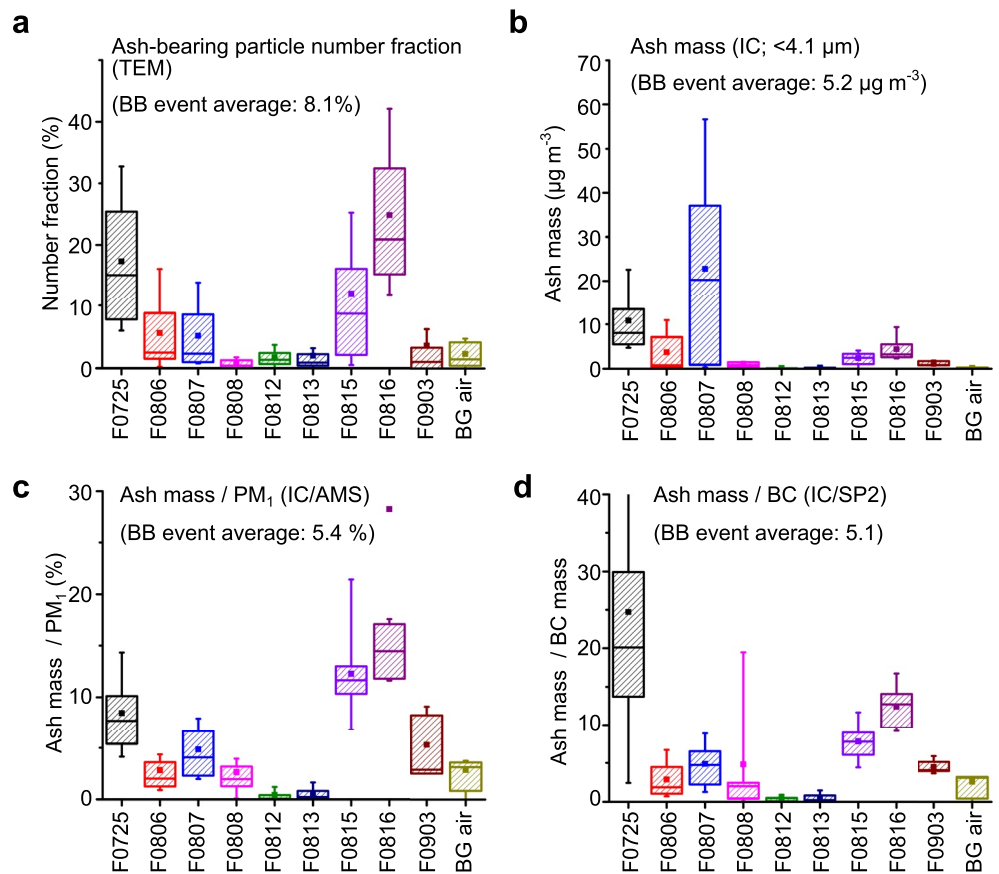


**Figure 9.** Average abundances of ash-bearing particles for the nine flights taken during the FIREX-AQ campaign. (a) Number fractions of ash-bearing particles determined by using TEM. (b) Fine ash mass concentrations ( $<4.1 \mu\text{m}$ ) measured by IC. (c) Fine ash mass relative to  $\text{PM}_{10}$  measured by an AMS (%). (d) Fine ash mass relative to BC mass from SP2 data. The ash mass was determined from the sum of the masses of  $\text{Mg}^{2+}$  and  $\text{Ca}^{2+}$  by assuming that they were carbonate. Agricultural burning samples were collected during the September 3 flight (F0903). The samples collected outside of visible plumes at low CO and particle concentrations were defined as background (BG) air samples, although some of these may be slightly influenced by dilute regional haze of aged smoke. The average values of each BB event are shown in each panel. The wide boxes, whiskers, and squares indicate the 25th, 50th, and 75th percentile ranges, 10th–90th percentile ranges, and average values, respectively.

and intensity, ground wind speed, and updraft strength all influenced ash production and transport in BB smoke. The study-average mean number fractions of ash-bearing particles within the BB smoke samples collected during the BBOP and MILAGRO campaigns were within the range of fire-specific number fractions from the FIREX-AQ campaign: 1.4% and 9.2%, respectively (Figure 10). The number fraction of ash-bearing particles in BB smoke did not clearly show either decreasing or increasing trends for up to 4 hr after emission or within  $\sim 100$  km from the emission sources in the FIREX-AQ samples (Figure 11). The ash-bearing particle number fraction was relatively high at an altitude of  $\sim 4,000$  m, where most of the BB smoke samples were collected (Figure 12).

Size distributions of ash-bearing particles peaked at  $\sim 800$  nm in area-equivalent diameter for samples from the FIREX-AQ and BBOP campaigns and at  $\sim 300$ – $1,000$  nm for those from the MILAGRO campaign (Figures 6–8 and S10 in Supporting Information S1). The size distributions of ash-bearing particles were several orders of magnitude smaller than those in previous reports of biomass bottom ash particles, which generally have median particle diameters of  $10$ – $1,000 \mu\text{m}$  (Bodí et al., 2014).

### 3.2. Composition of Ash-Bearing Particles

The Ca and Mg species in ash-bearing particles mostly consist of carbonates, oxalates, oxides, hydroxides, phosphates, chlorides, sulfates, or their mixtures (Figures 3, 4 and S2–S5 in Supporting Information S1). Specific ash

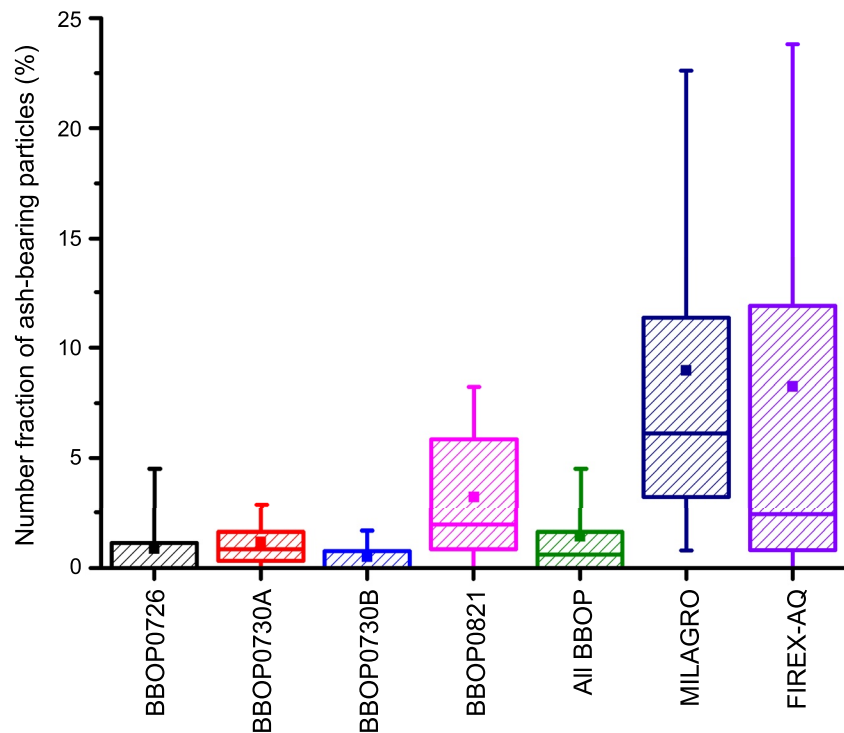


**Figure 10.** Number fractions of ash-bearing particles from samples obtained during the BBOP, MILAGRO, and FIREX-AQ campaigns (all BB samples, including those from wildfires and agricultural fires). The wide boxes, whiskers, and squares indicate the 25th, 50th, and 75th percentile ranges, 10th–90th percentile ranges, and average values, respectively. The numbers of TEM samples are 15; 15; 15; 14; 59; 10; and 208 from left to right.

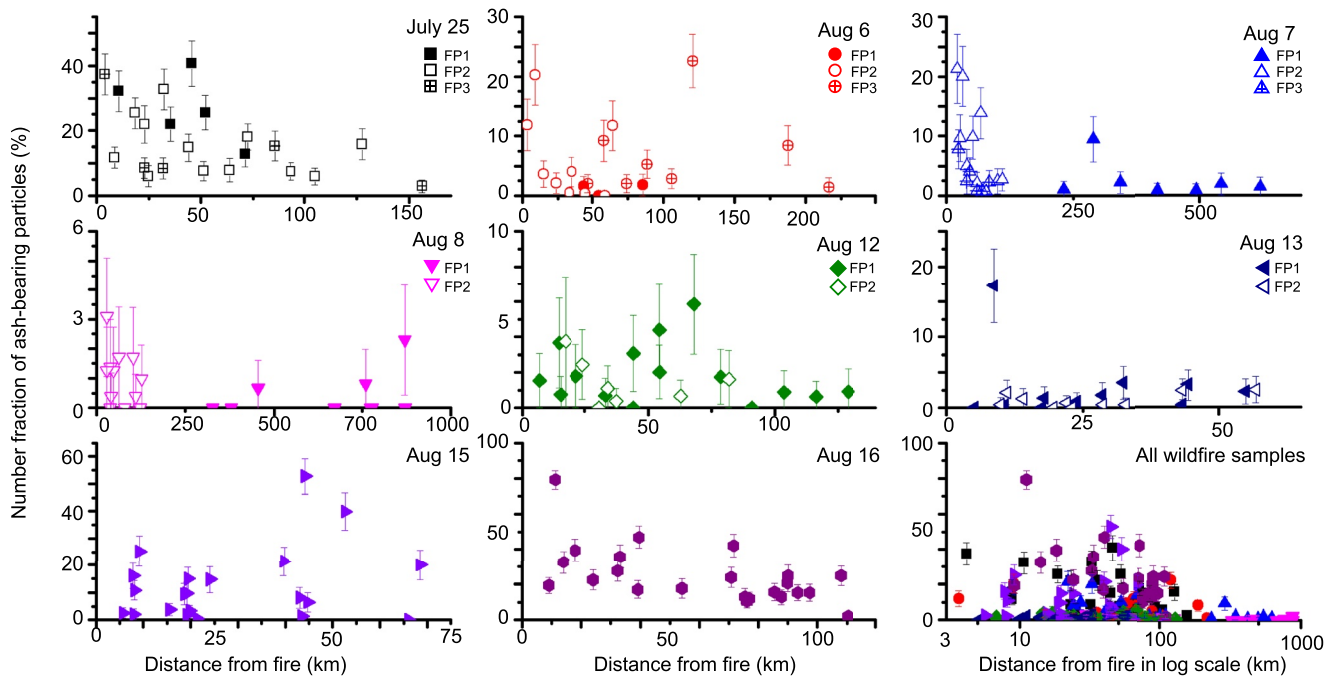


**Figure 11.** Ash-bearing particle number fractions vs. distance from fire sources for wildfire samples obtained during the FIREX-AQ campaign. The physical transport hours are approximately 10 hr for ~200 km and approximately two days for 900 km (maximum). Scales for x- and y-axes differ depending on the flights. Flights from July 25 to August 13 had two or three repeated flight patterns (FP), which are shown using different symbols in each panel. The panel “All wildfire smoke” uses single symbols for each flight and is shown in a log scale. Uncertainties are reported as 95% confidence intervals.

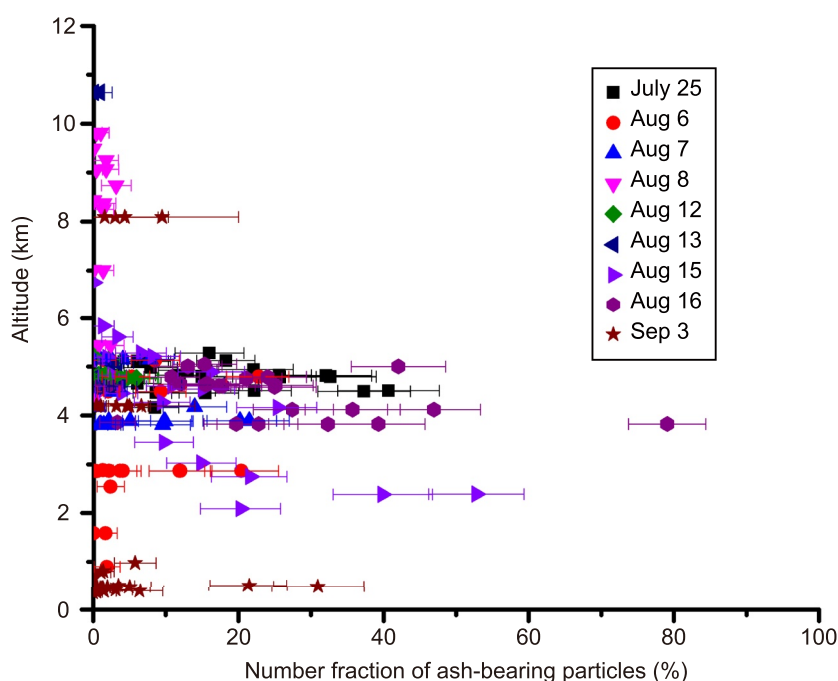


**Figure 12.** Ash-bearing particle number fractions at the median sampling altitude above mean sea level. The altitudes were measured by the DC8 navigation system (<https://www-air.larc.nasa.gov/missions/firex-aq/index.html>; last access on June 18, 2021). Uncertainties are reported as 95% confidence intervals.

particle compositions depend on the formation temperature (Bodí et al., 2014). For example, at fire temperatures below  $\sim 450^{\circ}\text{C}$ , ash particles occur as organic-rich ash or oxalates (e.g.,  $\text{CaC}_2\text{O}_4$ ), whereas at  $\sim 500^{\circ}\text{C}$ , oxalate is converted into carbonate (e.g.,  $\text{CaCO}_3$ ). At still higher temperature ( $>580^{\circ}\text{C}$ ), the carbonate is converted to calcium oxide (e.g.,  $\text{CaO}$ ). From interactions with water vapor in the atmosphere, calcium oxide becomes the hydroxide ( $\text{Ca(OH)}_2$ ). Although ash particles are mixtures of these components, the atomic ratio between O and  $\text{Mg} + \text{Ca}$  ( $\text{O}/(\text{Mg} + \text{Ca})$ ) is nearly three (Figure S11 in Supporting Information S1), suggesting that carbonates are likely the dominant form in the ash particles. A heating experiment in the vacuum TEM chamber without oxygen also suggested that the ash-bearing particles were refractory materials at  $<800^{\circ}\text{C}$ , consistent with calcium carbonate (Text S3 in Supporting Information S1).

The average weight % of Mg, P, and Ca among all particles measured by TEM was closely related to the ash-bearing particle number fractions ( $R^2 > 0.5$ ; Figure 13). Our TEM study indicated that these elements were significant components of fine ash particles (Figures 3 and 4). Raison et al. (1985) also showed that these elements were  $>10$  times higher in ash compared to its original fuel (unburned litter). These results suggest that ash-bearing particles predominantly contributed to the proportions of Mg, P, and Ca in the BB samples. Other elements (e.g., Si, K, and Fe) also have weak relationships with ash-bearing particles among samples having high ash-bearing particle number fractions ( $>10\%$ ). Oxygen can originate from ash components, organic materials, and substrates. As a result, samples having little or no ash-bearing particles can have relatively high O wt% (Figure 13). Although ash-bearing particles contain C, C from organic materials has the dominant contribution, and the C weight % and ash-bearing particle number % show a negative relationship.

Although the qualitative compositions of the ash-bearing particles were similar among different BB events, their quantitative compositions depended on the source and particle size. For example, ash-bearing particles from agricultural burning had more Mg and P and less Ca than those from wildfires (Figure 14), showing that their composition is sensitive to the fuel type (Bodí et al., 2014; Misra et al., 1993). Additionally, compositions and shapes of ash-bearing particles depend on particle size, with larger particles having higher C and Al weight %. In comparison, smaller particles exhibited increases in the weight % of O, Mg, P, and Ca as well as in particle roundness (i.e., a decrease in the shape factor; Figure 15). This size dependence of ash-bearing particle composition observed in the present study possibly reflects differences in the original microstructures of ash particles. This

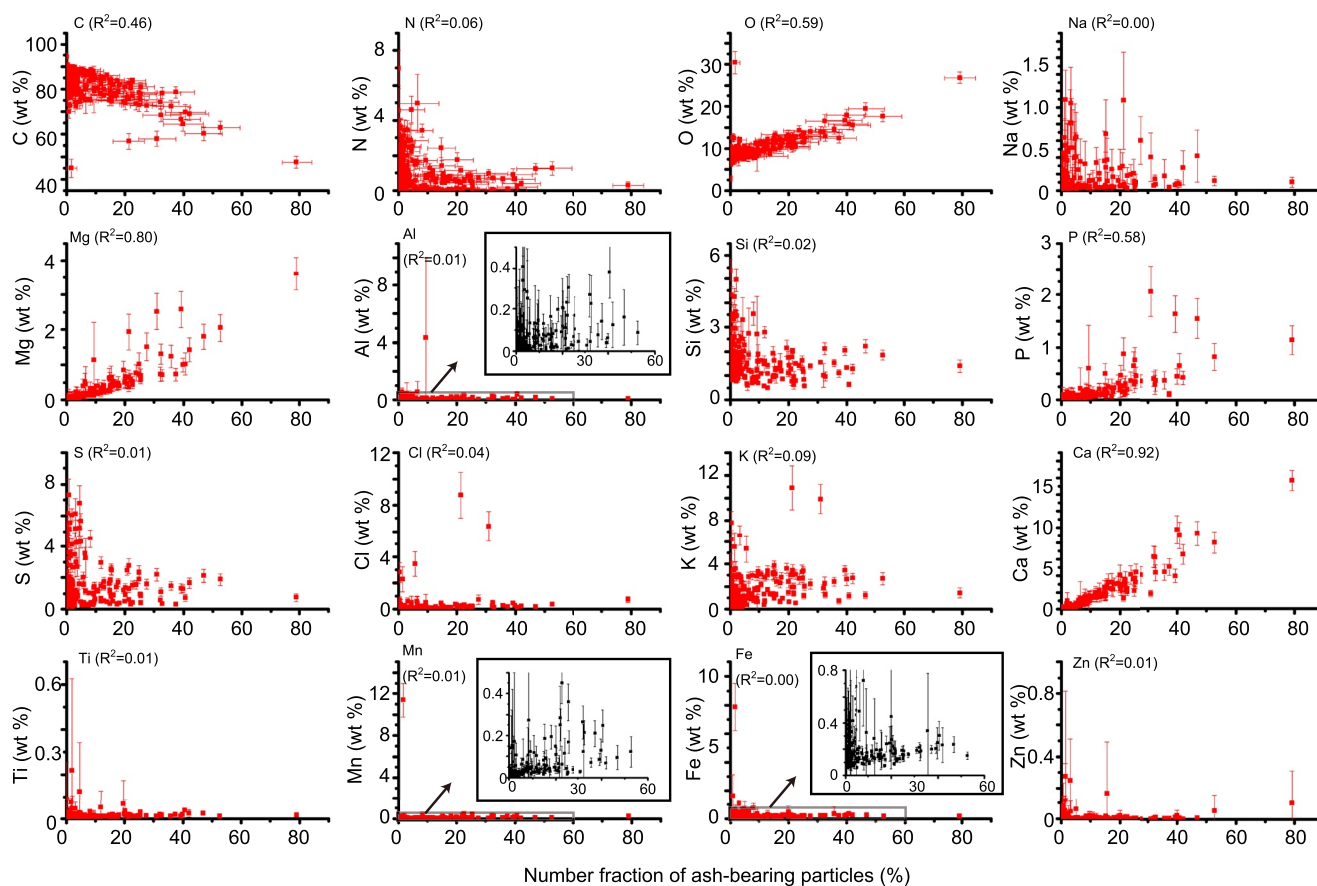


**Figure 13.** Relationship between the weight % and ash-bearing particle number fractions (%) for the FIREX-AQ samples. The insets for Al, Mn, and Fe enlarge the plots with small weight % values. Uncertainties are reported as 95% confidence intervals for 221 TEM samples.

interpretation is supported by laboratory-generated ash particles that show heterogeneous elemental distributions and structures (Figures 5 and S6 in Supporting Information S1), consistent with other biofuel ash particle studies (Kleinhans et al., 2018). When biofuels are combusted, organic components are burned or evaporated, leaving fibrous structures consisting of, for example, Ca, Mg, K, Al, or their mixtures, consistent with the chemical compositions of various biomass (Vassilev et al., 2010).

### 3.3. Hygroscopicity and Ice Nucleation Property of Ash-Bearing Particles

An environmental chamber with an optical microscope was used to evaluate the hygroscopicity and ice-nucleating activity of ash-bearing particles, critical parameters impacting the ability of ash-bearing particles to form cloud droplets and ice crystals. Concomitant with the increase in relative humidity (RH) inside the environmental chamber, the ash-bearing particles became spherical and increased in size due to water vapor uptake, that is, they deliquesced at RH values between 80% and 89% (Figure 16). This result suggests that ash-bearing particles can be efficiently activated as CCN and could also be removed from the atmosphere by precipitation. In the atmosphere, although Ca and Mg carbonates change compositions by reacting with acidic gases (e.g., nitric acid) and deliquesce, these nascent carbonate particles are not highly soluble in water (Guo et al., 2019; Tang et al., 2016). Therefore, water-soluble salts such as sulfates and potassium salts were possibly deliquesced in the measured ash-bearing particles. Following deliquescence, some small fragments were observed, suggesting that some insoluble fractions remained as nanosized grains (Figure 16).

The contributions of INPs from BB smoke are of interest as INPs also influence cloud formation and radiative forcing. Jahn et al. (2020) showed that ash particles are an important source of INPs in BB smoke in addition to mineral dust particles. Barry et al. (2021) also suggested a possible ash particle contribution

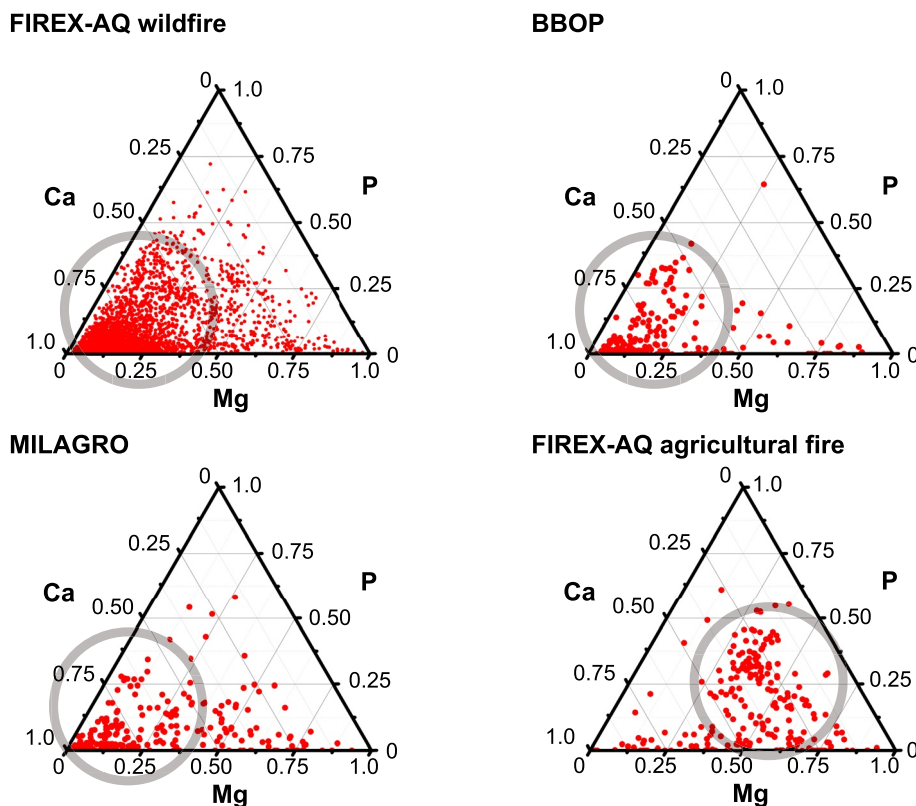


**Figure 14.** Differences of relative ash-bearing particle compositions (weight %) between wildfires and agricultural fires. Ternary plots among Ca, Mg, and P are shown for the three campaigns (wildfires) and the FIREX-AQ agricultural fire. The numbers of ash-bearing particles are 3,865; 183; 240; and 233 for the samples from the FIREX-AQ wildfire, BBOP, MILAGRO, and FIREX-AQ agricultural fire. Gray circles cover the dominant plotted areas.

to INP formation in smoke plumes from western US wildfires in 2018. To test the ice-nucleating ability of ash-bearing particles in our BB samples, we conducted ice-nucleating experiments by decreasing the sample temperature with saturated humidity using the same chamber used in the CCN experiment (Figure 17). Although this measurement is preliminary, it qualitatively identifies particles with a relatively high onset temperature for ice nucleation within the field of view. When the temperature around the TEM grid samples was decreased in the chamber, ice crystals developed over various particles (Figure 17). We measured the composition of particles that developed ice crystals at  $>-38^{\circ}\text{C}$  using STEM-TEM after the ice-nucleating experiments. In total, 21 particles from six samples were observed to develop ice crystals, nine ash-bearing particles, eight mineral dust-bearing particles, and four other particles. In these samples, the ash-bearing particle number fractions were much higher than those of mineral dust particles. Thus, the ice-nucleating efficiency of ash-bearing particles was weaker than that of mineral dust particles, but ash-bearing particles can still act as INPs in BB smoke. Other possible INPs from BB include tarballs and biological particles (Barry et al., 2021; McCluskey et al., 2014).

### 3.4. Emission Estimates of Fine Ash Aerosol Particles

During the FIREX-AQ campaign, the composition of soluble aerosol particles smaller than  $\sim 4.1\ \mu\text{m}$  in aerodynamic diameter was measured using IC. This measurement provides the soluble Mg and Ca concentrations in those particles in the sampled BB smoke and thus a quantitative evaluation of mass concentrations of ash components. Although mineral dust particles can contribute to the Ca and Mg concentrations, their number fractions are small in the BB smoke ( $\sim 0.2\%$ ; Figure 1), and they accounted for approximately 0.5% of all Ca and Mg masses observed in the FIREX-AQ TEM particles (Text S2 in Supporting Information S1). A comparison between the IC-determined Ca and Mg concentrations and TEM ash-bearing particle number fraction data also showed a good

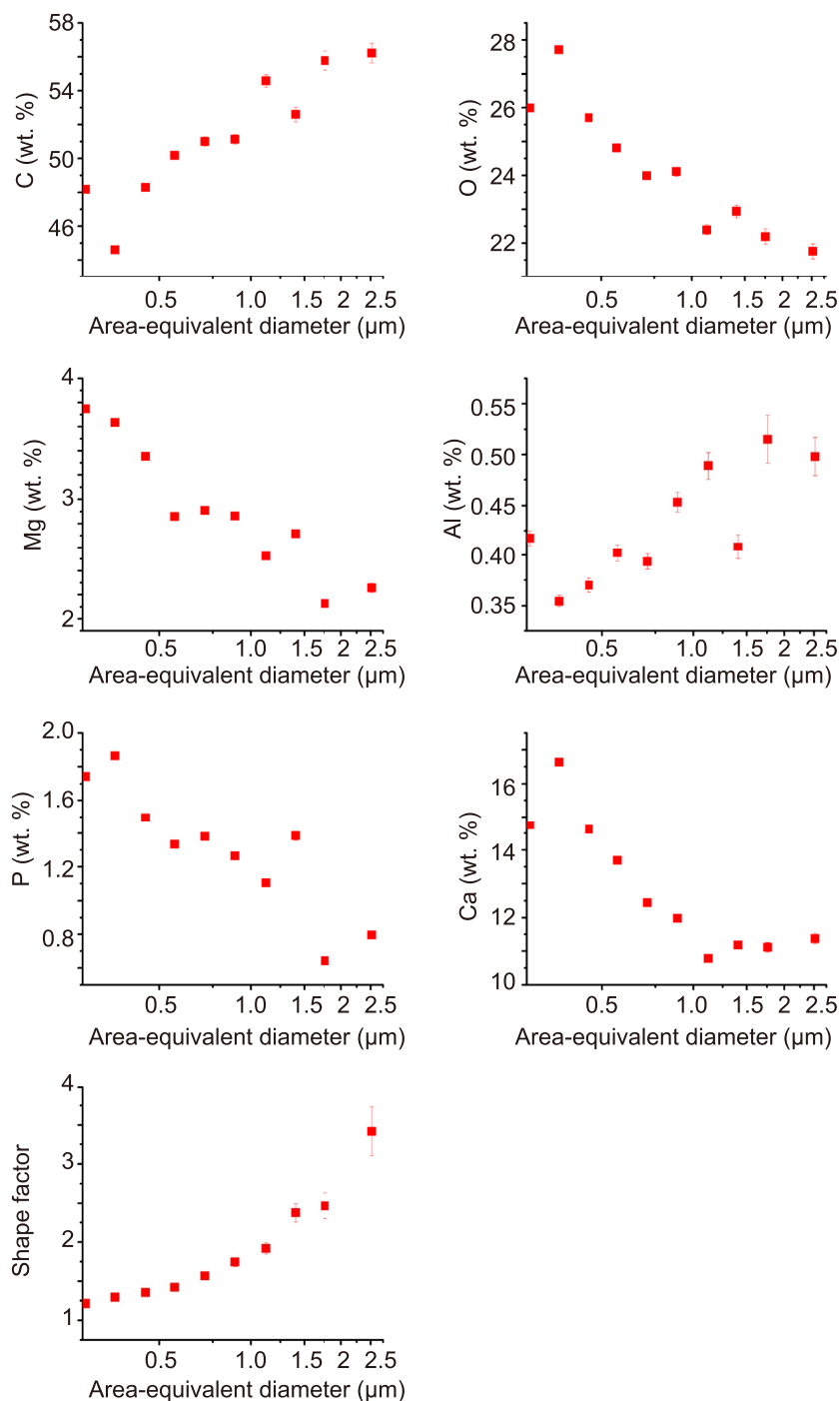


**Figure 15.** Changes in ash-bearing particle composition with size for particles collected during the FIREX-AQ campaign. The total number of ash-bearing particles is 4,098. Uncertainties are reported as 95% confidence intervals. Shape factors were obtained from a square of measured perimeters ( $P$ ) from binary STEM images divided by the spherical perimeters that are calculated from the area-equivalent diameters ( $d$ ):  $(P/(\pi d))^2$ . A sphere has a shape factor of 1, and a particle with a complicated shape has a shape factor higher than 1.

correlation (Figure 18). These results indicate that the Ca and Mg masses measured using the IC can be used to estimate the masses of the fine ash components. See Texts S1 and S2 in Supporting Information S1 for more discussion of mineral dust contributions and the IC and TEM comparison, respectively.

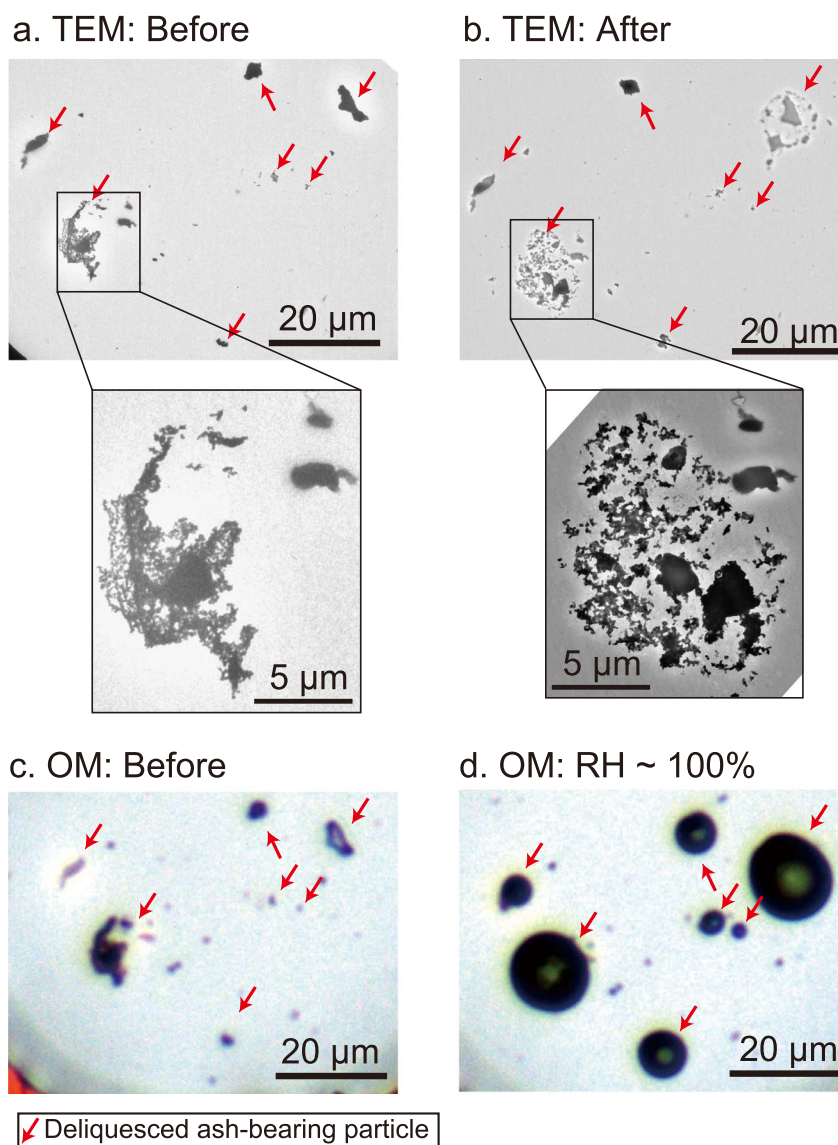


**Figure 16.** Hygroscopicity experiments on ash-bearing particles measured using an environmental chamber with an optical microscope. (a–b) TEM image of ash-bearing particles (a) before and (b) after the hygroscopicity experiment. Ash-bearing particles became fragments over the substrate after deliquescence (enlarged TEM images in panel (b)). The TEM image in (a) was taken before the hygroscopicity experiment with low magnifications and a weak beam current density to minimize the electron beam damage. (c and d) Optical microscope images show the changes in particle shapes with increasing RH. The sample was exposed to ~100% relative humidity (RH). These ash-bearing particles deliquesced at RH values between 80% and 89%. Red arrows indicate deliquesced ash-bearing particles. The sample was collected on July 24, 2019, during the FIREX-AQ campaign in coarse particle mode (aerodynamic diameter >700 nm in 50% cutoff size).

The average IC mass concentration of  $\text{Ca}^{2+} + \text{Mg}^{2+}$  was  $2.0 \mu\text{g m}^{-3}$  for all the FIREX-AQ smoke also sampled for TEM analysis. Under the assumptions that Ca and Mg occur as carbonates ( $\text{CaCO}_3$  and  $\text{MgCO}_3$ ) based on the TEM results (Figure S11 in Supporting Information S1) and can serve as proxies for ash components, we estimated that the ash concentration in our BB smoke samples was  $5.2 \mu\text{g m}^{-3}$  (Figure 9 and Table 4). This average mass concentration of fine ash components represents ~5% of the average PM1 measured using an AMS, 510% of the average accumulation-mode BC measured using a SP2, and 629% of the average K measured by IC (Table 4). The ash mass concentrations determined by IC are likely underestimated when considering their insoluble fractions, other minor elements within ash components (e.g., Al, Fe, and P), and the inlet cutoff size. Thus, the ash mass concentrations derived here are lower limits, and those in the atmosphere can be higher than those shown here. For reference, when assuming oxalate ( $\text{C}_2\text{O}_4^{2-}$ ), hydroxide ( $(\text{OH})_2^{2-}$ ), and oxide ( $\text{O}^{2-}$ ) forms, the ash concentra-



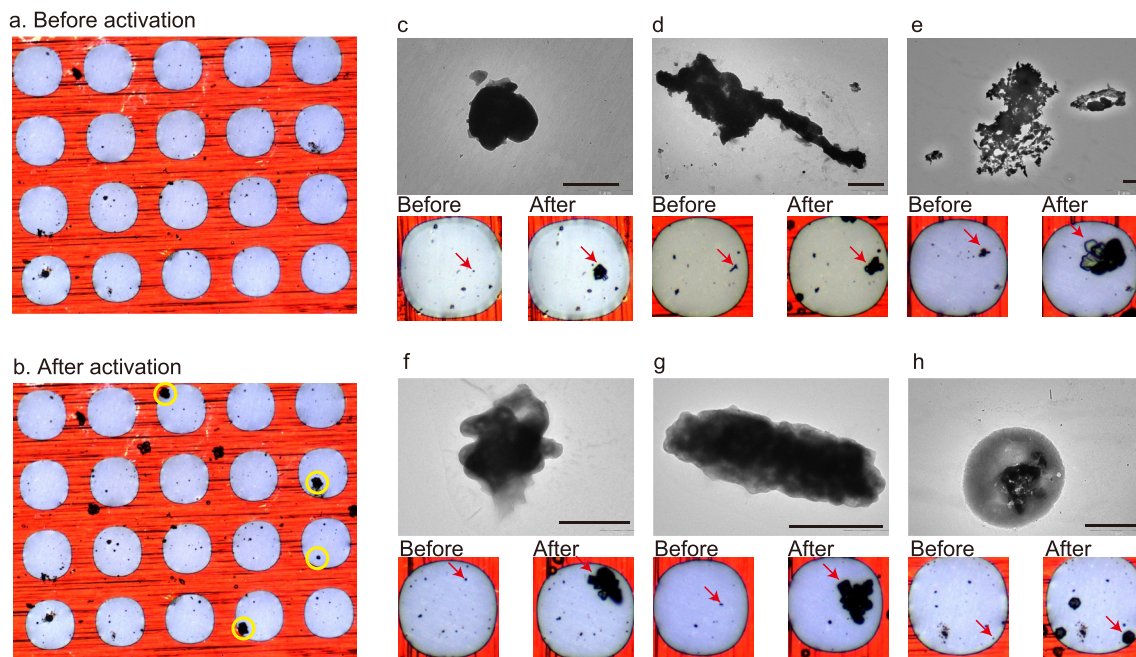


**Figure 17.** Ice nucleating particle (INP) activity experiments on ash-bearing particles measured using an environmental chamber with an optical microscope. (a–b) Optical microscope images before (a) and after (b) ice activation at  $-27^{\circ}\text{C}$  ( $\pm 3^{\circ}\text{C}$ ) with saturated water vapor (RH of 8.0% at the chamber temperature ( $17.6^{\circ}\text{C}$ )). Particles that had ice crystals over the Formvar substrate are marked with yellow circles (b). The sample was collected on August 17, 2019 at 02:33. (c–h) Examples of TEM (upper; after activation) and optical microscopy images (lower; before and after activation) of ash-bearing particles that became INPs at  $> -38^{\circ}\text{C}$ . Sampling times were July 24 (c) and August 17, 2019 (d–h). The onset temperatures are  $-31^{\circ}\text{C}$ ,  $-31^{\circ}\text{C}$ ,  $-35^{\circ}\text{C}$ ,  $-35^{\circ}\text{C}$ ,  $-35^{\circ}\text{C}$ ,  $-35^{\circ}\text{C}$ , and  $-31^{\circ}\text{C}$  for particles (c–h), respectively. Red arrows indicate activated ash-bearing particles. Scale bars indicate  $1\ \mu\text{m}$ .

tions become  $\sim 6.8$ ,  $3.8$ , and  $2.8\ \mu\text{g m}^{-3}$ , which are approximately 130%, 72%, and 52% of the values from the carbonate assumption, respectively.

As BB emissions influence the global climate, we estimate the scale of global emissions of fine ash mass ( $< \sim 4.1\ \mu\text{m}$ ). To assess global fine ash emissions, we used our measured amounts of fine ash mass relative to BC and K, which are widely used as BB tracers, along with the global BB emission inventories of BC and K estimated by Andreae (2019) and the BB BC emission inventories that are commonly used in climate models. Estimates of annual global BB BC emission range from  $1.73$  to  $3.20\ \text{Tg yr}^{-1}$ , and that of K is  $2.1\ \text{Tg yr}^{-1}$  (Table S1 in Supporting Information S1).

Assuming that the ratios ash/BC and ash/K in our measurements are representative of BB emissions, the global emissions of ash components in BB aerosol particles are estimated to be  $11.6\ \text{Tg yr}^{-1}$  with a range between  $8.8$  and  $16.3$  depending on BC and K inventories (Table 5). In addition to the annual fine ash emission estimate, we used the BC emission inventory to evaluate the daily emissions of fine ash mass during the FIREX-AQ campaign from July 22 to August 19, 2019 in the observed area ( $34.0$ – $49.0^{\circ}\text{N}$ ,  $112.0$ – $119.0^{\circ}\text{W}$ ; Table 5). This estimate provides daily emission data from the same area and sampling periods of BB events observed during the FIREX-AQ campaign. The fine ash daily emission was estimated to be  $99\ \text{g km}^{-2}\ \text{day}^{-1}$ . These values have  $\sim 100\%$  uncertainty ranges based on the observed fire-fire variability (Table 4), and noting that some large ash-bearing particles ( $> \sim 4.1\ \mu\text{m}$ ) can also be transported long distances from the BB sources. The representativeness of the FIREX-AQ BB smoke within global BB is also a source of uncertainty. For example, the emission factors of BC in western US wildfires are reported to be  $0.389 \pm 0.17\ \text{g kg}^{-1}$  (Permar et al., 2021) and  $0.18 \pm 0.08\ \text{g kg}^{-1}$  (Selimovic et al., 2020), which are similar to or smaller than those in savanna or tropical forest ( $0.37 \pm 0.20$  and  $0.52 \pm 0.28\ \text{g kg}^{-1}$ , respectively; Akagi et al., 2011). Our ash number fraction average for tropical BB in MILA-GRO was also similar to that of FIREX-AQ (Figure 10). For reference, an approximate emission factor for ash from wildfires can be calculated from the data above as  $\sim 1.5 \pm 1.0\ \text{g kg}^{-1}$ . Investigations of ash-bearing particle emissions from various BBs at a global scale are strongly recommended for future studies. In summary, although the uncertainty range is large, our first ash emissions estimates suggest that the global emission of fine ash mass

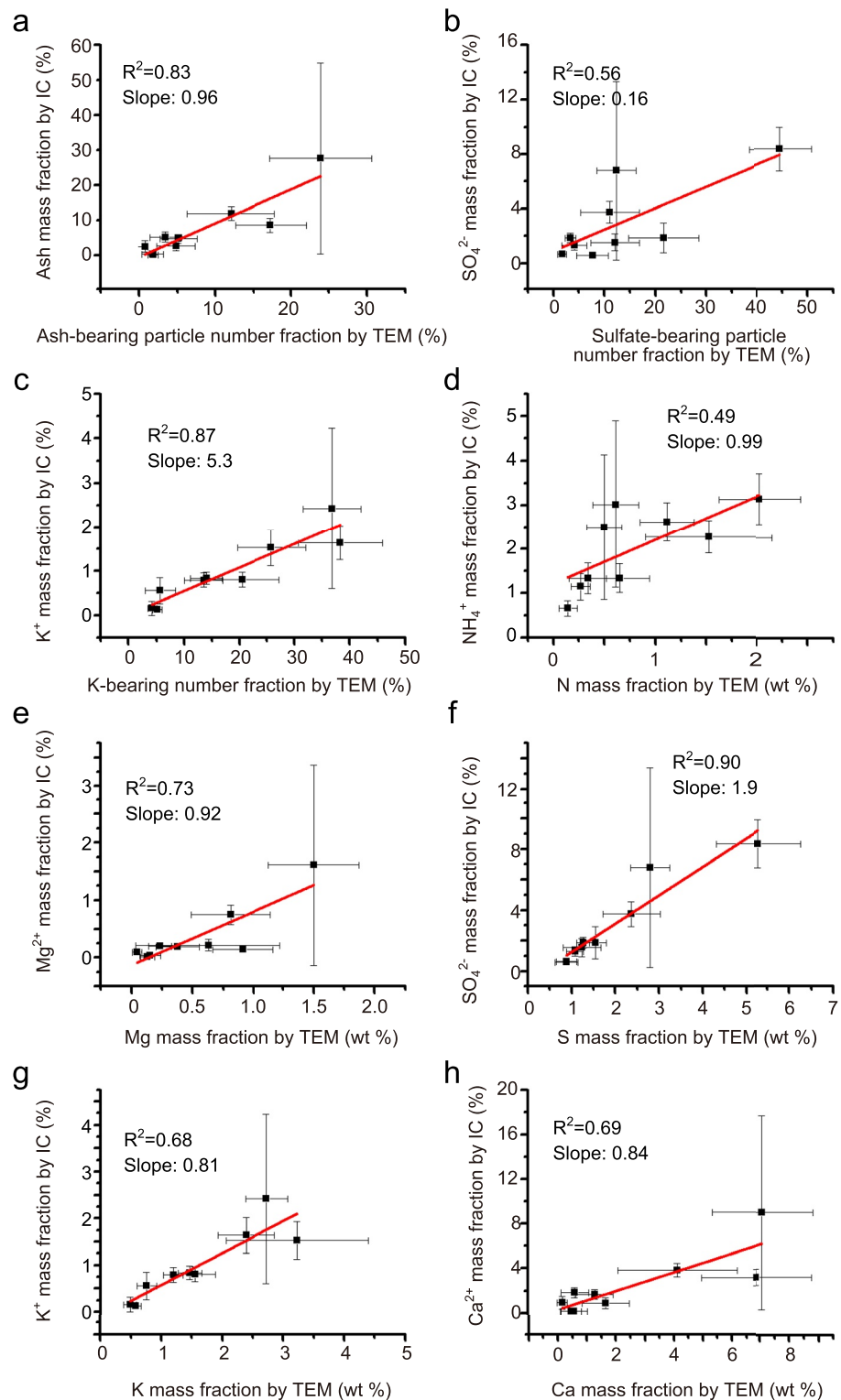


**Figure 18.** Relationship between the ion chromatography (IC) and TEM results for each flight average during the FIREX-AQ campaign (nine flights). The IC and TEM sampling periods cover the same smoke transects with slightly different start and stop times. Mass fraction (wt %) for each element in the TEM data (x-axes) was determined by dividing the mass of each element by the sum of all measured elements and is the averaged values of BB samples for each flight. Mass fractions (wt %) of IC data (y-axes) were obtained from IC mass concentrations divided by the  $\text{PM}_{10}$  mass measured by AMS. Uncertainties for the IC and TEM measurements are reported as 95% confidence intervals.

**Table 4**  
Average Concentrations of Each Component Observed During FIREX-AQ

	$\mu\text{g m}^{-3}$	(%) <sup>c</sup>
Fine ash	$5.15^a \pm 4.94^b$	100
K	$0.82 \pm 0.78$	$629 \pm 852$
BC	$1.01 \pm 0.84$	$510 \pm 647$
PM <sub>1</sub>	$95.3 \pm 78.2$	$5 \pm 7$

<sup>a</sup>The values are averaged within TEM sample periods from each BB event.

<sup>b</sup>Error ranges are 95% confidence intervals. <sup>c</sup>Percent values are the ash mass relative to each component (%).

from BB is considerable, that is, ash might be the second-largest component of aerosols in BB smoke by mass after organic carbon (Andreae, 2019), and fine ash should be treated as a major aerosol component in BB smoke.

### 3.5. Implications for Climate, Mineral Dust Measurements, and Human Health

Ash-bearing particles can serve as CCN and INPs (Jahn et al., 2020; Umo et al., 2015) and thus contribute to cloud formation and radiative properties. Their compositions indicate that these ash particles mainly scatter light (Al Omari et al., 2016) and therefore have a negative direct radiative forcing effect at short wavelengths. On the other hand, ash particles are commonly found to be mixed with organic materials and soot (Figure 3), raising the potential for influencing the optical properties of light-absorbing particles

such as soot and potentially brown carbon. These mixtures with light-absorbing particles should also be considered to understand the impacts of ash components on the net optical properties of BB emissions and hence on BB radiative forcing.

As Ca is often used as a tracer of mineral dust and soil particles in aerosol and ice core samples (Laskin et al., 2005; Ruth et al., 2008), it is possible that some ash particles have been misidentified as mineral dust or soil particles in other chemical analyses including those from large surface monitoring network such as the Interagency Monitoring of Protected Visual Environments (Malm et al., 1994). In addition, satellite observations have also potentially misidentified some ash as mineral dust because ash particles and mineral dust particles both have nonspherical shapes with similar optical properties, resulting in overestimates of mineral dust particles. Thus, identifying ash particles will improve BB measurements in various samples, including aerosol particles and ice cores.

The small sizes of ash-bearing particles suggest that they are inhalable by humans; that is, based on their size distribution, ~10%–20% of ash-bearing particles can be inhaled and deposited in the lungs (Londahl et al., 2008). Particulate matter from BB has been reported to be toxic to humans (Pardo et al., 2020; C. E. Reid et al., 2016). BB toxicity has been attributed to organic materials, but some ash-bearing particles may also indirectly contribute to the toxicity (Harper et al., 2019). Following dissolution, nanosized ash fragments (Figure 16) may more easily travel deeper into the body (Oberdörster et al., 2005) than the original ash-bearing particles. Since BB severely influences the air quality of residential areas globally, further study is recommended regarding ash influences on human health based on the physical and chemical properties of fine ash-bearing particles shown in this study.

## 4. Conclusions

This study revealed compositions, shapes, sizes, and hygroscopicity of ash-bearing particles with diameters smaller than several microns from various BB smokes and quantified their number fractions and mass concentrations using TEM and IC, respectively. Due to their small sizes, these ash-bearing particles can be transported long distances across the globe, influencing cloud formations and the radiative balance and be inhaled in the human body. Their estimated global emission ( $11.6 \text{ Tg yr}^{-1}$ ) suggests that ash components can be a major component in aerosol particles from BB. As our emission estimate of ash components includes large uncertainties, further measurements and global emission estimations are strongly recommended. We suggest that ash components should be explicitly considered as a category of BB aerosol in BB observations and models.

**Table 5**  
Estimates of Fine Ash Mass Emissions ( $<4.1 \mu\text{m}$ )

	GFAS	GFED	CMIP6	Andreae BC	Andreae K	Average
Global ( $\text{Tg yr}^{-1}$ )	9.3	10.2	8.8	16.3	13.2	11.6
North America ( $\text{g km}^{-2} \text{ day}^{-1}$ )	126	73	NA	NA	NA	99

Note. NA, not available.

## Data Availability Statement

FIREX-AQ data are available at <https://www-air.larc.nasa.gov/cgi-bin/ArcView/firexaq>. BBOP data are available at <https://www.arm.gov/research/campaigns/aaf2013bbop>. STEM-EDS data for all individual particles and those for TEM sample average are available at <https://10.5281/zenodo.5112760>.

## Acknowledgments

The authors acknowledge the science team members, supporting staff, and the pilots and flight staff of the research aircraft for FIREX-AQ (NASA DC8), BBOP (DOE G-1), and MILAGRO (Forest Service Twin Otter). The authors thank Duli Chand and John Hubbe (PNNL) for the G-1 sampling. The BBOP campaign was supported by the ARM user facility, a US DOE Office of Science user facility managed by the Office of Biological and Environmental Research. The MILAGRO campaign was supported by the NSF grant 0513055. KA, NO, and MK thank the Environmental Research and Technology Development Fund (JPMEERF20202003, JPMEERF20205001, JPMEERF20172003, JPMEERF20215003, and JPMEERF20165005) of the Environmental Restoration and Conservation Agency of Japan, the Global Environmental Research Coordination System from the Ministry of the Environment of Japan (MLIT1753), the Arctic Challenge for Sustainability II (ArCS II; JP-MXD1420318865), and the Japan Society for the Promotion of Science (JSPS) KAKENHI program (grant numbers JP16K16188, JP18H03363, JP18H05292, JP19H01972, JP19H04236, JP19K21905, and JP19H04259) for financial support. This study was also supported by NASA grants 80NSSC19K0124, 80NSSC18K0630 (HG, PCJ, and JLL), and 80NSSC18K0631 (ES and JED) and by NOAA Grant NA16OAR4310100 (RJY).

## References

- Abatzoglou, J. T., & Williams, A. P. (2016). Impact of anthropogenic climate change on wildfire across western US forests. *Proceedings of the National Academy of Sciences*, *113*(42), 11770–11775. <https://doi.org/10.1073/pnas.1607171113>
- Adachi, K., & Buseck, P. R. (2008). Internally mixed soot, sulfates, and organic matter in aerosol particles from Mexico City. *Atmospheric Chemistry and Physics*, *8*(21), 6469–6481. <https://doi.org/10.5194/acp-8-6469-2008>
- Adachi, K., Oshima, N., Ohata, S., Yoshida, A., Moteki, N., & Koike, M. (2021). Compositions and mixing states of aerosol particles by aircraft observations in the Arctic springtime, 2018. *Atmospheric Chemistry and Physics*, *21*, 3607–3626. <https://doi.org/10.5194/acp-21-3607-2021>
- Adachi, K., Sedlacek, A. J., Kleinman, L., Chand, D., Hubbe, J. M., & Buseck, P. R. (2018). Volume changes upon heating of aerosol particles from biomass burning using transmission electron microscopy. *Aerosol Science and Technology*, *52*(1), 46–56. <https://doi.org/10.1080/02786826.2017.1373181>
- Adachi, K., Sedlacek, A. J., Kleinman, L., Springston, S. R., Wang, J., Chand, D., et al. (2019). Spherical tarball particles form through rapid chemical and physical changes of organic matter in biomass-burning smoke. *Proceedings of the National Academy of Sciences*, *116*(39), 19336–19341. <https://doi.org/10.1073/pnas.1900129116>
- Akagi, S. K., Yokelson, R. J., Wiedinmyer, C., Alvarado, M. J., Reid, J. S., Karl, T., et al. (2011). Emission factors for open and domestic biomass burning for use in atmospheric models. *Atmospheric Chemistry and Physics*, *11*(9), 4039–4072. <https://doi.org/10.5194/acp-11-4039-2011>
- Al Omari, M. M., Rashid, I. S., Qinna, N. A., Jaber, A. M., & Badwan, A. A. (2016). Calcium carbonate. *Profiles of Drug Substances, Excipients, and Related Methodology*, *41*, 31–132. <https://doi.org/10.1016/bs.podrm.2015.11.003>
- Andreae, M. O. (2019). Emission of trace gases and aerosols from biomass burning—An updated assessment. *Atmospheric Chemistry and Physics*, *19*(13), 8523–8546. <https://doi.org/10.5194/acp-19-8523-2019>
- Andreae, M. O., Rosenfeld, D., Artaxo, P., Costa, A. A., Frank, G. P., Longo, K. M., & Silva-Dias, M. A. F. (2004). Smoking rain clouds over the Amazon. *Science*, *303*(5662), 1337–1342. <https://doi.org/10.1126/science.1092779>
- Barry, K. R., Hill, T. C. J., Levin, E. J. T., Twohy, C. H., Moore, K. A., Weller, Z. D., et al. (2021). Observations of ice nucleating particles in the free troposphere from western US wildfires. *Journal of Geophysical Research: Atmospheres*, *126*(3). <https://doi.org/10.1029/2020jd033752>
- Bodi, M. B., Martin, D. A., Balfour, V. N., Santin, C., Doerr, S. H., Pereira, P., et al. (2014). Wildland fire ash: Production, composition, and eco-hydro-geomorphic effects. *Earth-Science Reviews*, *130*, 103–127. <https://doi.org/10.1016/j.earscirev.2013.12.007>
- Brocchi, V., Krystzofiak, G., Catoire, V., Guth, J., Maréchal, V., Zbinden, R., et al. (2018). Intercontinental transport of biomass burning pollutants over the Mediterranean Basin during the summer 2014 ChArMEX-GLAM airborne campaign. *Atmospheric Chemistry and Physics*, *18*, 6887–6906. <https://doi.org/10.5194/acp-18-6887-2018>
- Brock, C. A., Cozic, J., Bahreini, R., Froyd, K. D., Middlebrook, A. M., McComiskey, A., et al. (2011). Characteristics, sources, and transport of aerosols measured in spring 2008 during the aerosol, radiation, and cloud processes affecting Arctic Climate (ARCPAC) Project. *Atmospheric Chemistry and Physics*, *11*(6), 2423–2453. <https://doi.org/10.5194/acp-11-2423-2011>
- Canagaratna, M. R., Jayne, J. T., Jimenez, J. L., Allan, J. D., Alfarra, M. R., Zhang, Q., et al. (2007). Chemical and microphysical characterization of ambient aerosols with the aerodyne aerosol mass spectrometer. *Mass Spectrometry Reviews*, *26*(2), 185–222. <https://doi.org/10.1002/mas.20115>
- Crutzen, P. J., & Andreae, M. O. (1990). Biomass burning in the tropics: Impact on atmospheric chemistry and biogeochemical cycles. *Science*, *250*(4988), 1669–1678. <https://doi.org/10.1126/science.250.4988.1669>
- DeCarlo, P. F., Kimmel, J. R., Trimborn, A., Northway, M. J., Jayne, J. T., Aiken, A. C., et al. (2006). Field-deployable, high-resolution, time-of-flight aerosol mass spectrometer. *Analytical Chemistry*, *78*(24), 8281–8289. <https://doi.org/10.1021/ac061249n>
- Dennison, P. E., Brewer, S. C., Arnold, J. D., & Moritz, M. A. (2014). Large wildfire trends in the western United States, 1984–2011. *Geophysical Research Letters*, *41*(8), 2928–2933. <https://doi.org/10.1002/2014gl059576>
- Eyring, V., Bony, S., Meehl, G. A., Senior, C. A., Stevens, B., Stouffer, R. J., & Taylor, K. E. (2016). Overview of the Coupled Model Inter-comparison Project Phase 6 (CMIP6) experimental design and organization. *Geoscientific Model Development*, *9*(5), 1937–1958. <https://doi.org/10.5194/gmd-9-1937-2016>
- Gidden, M. J., Riahi, K., Smith, S. J., Fujimori, S., Luderer, G., Kriegler, E., et al. (2019). Global emissions pathways under different socio-economic scenarios for use in CMIP6: A data set of harmonized emissions trajectories through the end of the century. *Geoscientific Model Development*, *12*(4), 1443–1475. <https://doi.org/10.5194/gmd-12-1443-2019>
- Guo, L., Gu, W., Peng, C., Wang, W., Li, Y. J., Zong, T., et al. (2019). A comprehensive study of hygroscopic properties of calcium- and magnesium-containing salts: Implication for hygroscopicity of mineral dust and sea salt aerosols. *Atmospheric Chemistry and Physics*, *19*(4), 2115–2133. <https://doi.org/10.5194/acp-19-2115-2019>
- Harper, A. R., Santin, C., Doerr, S. H., Froyd, C. A., Albini, D., Otero, X. L., et al. (2019). Chemical composition of wildfire ash produced in contrasting ecosystems and its toxicity to *Daphnia magna*. *International Journal of Wildland Fire*, *28*(10), 726. <https://doi.org/10.1071/wf18200>
- Hecobian, A., Liu, Z., Hennigan, C. J., Huey, L. G., Jimenez, J. L., Cubison, M. J., et al. (2011). Comparison of chemical characteristics of 495 biomass burning plumes intercepted by the NASA DC-8 aircraft during the ARCTAS/CARB-2008 field campaign. *Atmospheric Chemistry and Physics*, *11*(24), 13325–13337. <https://doi.org/10.5194/acp-11-13325-2011>
- Heim, E. W., Dibb, J., Scheuer, E., Jost, P. C., Nault, B. A., Jimenez, J. L., et al. (2020). Asian dust observed during KORUS-AQ facilitates the uptake and incorporation of soluble pollutants during transport to South Korea. *Atmospheric Environment*, *224*, 117305. <https://doi.org/10.1016/j.atmosenv.2020.117305>
- Hirsch, E., & Koren, I. (2021). Record-breaking aerosol levels explained by smoke injection into the stratosphere. *Science*, *371*(6535), 1269–1274. <https://doi.org/10.1126/science.abe1415>
- Hodzic, A., Campuzano-Jost, P., Bian, H., Chin, M., Colarco, P. R., Day, D. A., et al. (2020). Characterization of organic aerosol across the global remote troposphere: A comparison of ATom measurements and global chemistry models. *Atmospheric Chemistry and Physics*, *20*, 4607–4635. <https://doi.org/10.5194/acp-20-4607-2020>

- Hudson, P. K., Murphy, D. M., Cziczko, D. J., Thomson, D. S., de Gouw, J. A., Warneke, C., et al. (2004). Biomass-burning particle measurements: Characteristic composition and chemical processing. *Journal of Geophysical Research*, *109*, D23S27. <https://doi.org/10.1029/2003JD004398>
- Jahn, L. G., Polen, M. J., Jahl, L. G., Brubaker, T. A., Somers, J., & Sullivan, R. C. (2020). Biomass combustion produces ice-active minerals in biomass-burning aerosol and bottom ash. *Proceedings of the National Academy of Sciences*, *117*(36), 21928–21937. <https://doi.org/10.1073/pnas.1922128117>
- Jöller, M., Brunner, T., & Obernberger, I. (2005). Modeling of aerosol formation during biomass combustion in grate furnaces and comparison with measurements. *Energy & Fuels*, *19*(1), 311–323. <https://doi.org/10.1021/ef049904m>
- Kaiser, J. W., Heil, A., Andreae, M. O., Benedetti, A., Chubarova, N., Jones, L., et al. (2012). Biomass burning emissions estimated with a global fire assimilation system based on observed fire radiative power. *Biogeosciences*, *9*(1), 527–554. <https://doi.org/10.5194/bg-9-527-2012>
- Kganyago, M., & Shikwambana, L. (2020). Assessment of the characteristics of recent major wildfires in the USA, Australia, and Brazil in 2018–2019 using multi-source satellite products. *Remote Sensing*, *12*(11), 1803. <https://doi.org/10.3390/rs12111803>
- Kleinhans, U., Wieland, C., Frandsen, F. J., & Spliethoff, H. (2018). Ash formation and deposition in coal and biomass fired combustion systems: Progress and challenges in the field of ash particle sticking and rebound behavior. *Progress in Energy and Combustion Science*, *68*, 65–168. <https://doi.org/10.1016/j.pecs.2018.02.001>
- Kleinman, L. I., Sedlacek, A. J., Adachi, K., Buseck, P. R., Collier, S., & Dubey, M. K., et al. (2020). Rapid evolution of aerosol particles and their optical properties downwind of wildfires in the western US. *Atmospheric Chemistry and Physics*, *20*(21), 13319–13341. <https://doi.org/10.5194/acp-20-13319-2020>
- Laskin, A., Wietsma, T. W., Krueger, B. J., & Grassian, V. H. (2005). Heterogeneous chemistry of individual mineral dust particles with nitric acid: A combined CCSEM/EDX, ESEM, and ICP-MS study. *Journal of Geophysical Research: Atmospheres*, *110*(D10). <https://doi.org/10.1029/2004JD005206>
- Li, J., Pósfai, M., Hobbs, P. V., & Buseck, P. R. (2003). Individual aerosol particles from biomass burning in southern Africa: 2. Compositions and aging of inorganic particles. *Journal of Geophysical Research: Atmospheres*, *108*(D13). <https://doi.org/10.1029/2002jd002310>
- Londahl, J., Pagels, J., Boman, C., Swietlicki, E., Massling, A., Rissler, J., et al. (2008). Deposition of biomass combustion aerosol particles in the human respiratory tract. *Inhalation Toxicology*, *20*(10), 923–933. <https://doi.org/10.1080/08958370802087124>
- Malm, W. C., Sisler, J. F., Huffman, D., Eldred, R. A., & Cahill, T. A. (1994). Spatial and seasonal trends in particle concentration and optical extinction in the United States. *Journal of Geophysical Research*, *99*(D1), 1347–1370. <https://doi.org/10.1029/93JD02916>
- McClure, C. D., & Jaffe, D. A. (2018). US particulate matter air quality improves except in wildfire-prone areas. *Proceedings of the National Academy of Sciences*, *115*(31), 7901–7906. <https://doi.org/10.1073/pnas.1804353115>
- McCluskey, C. S., DeMott, P. J., Prenni, A. J., Levin, E. J. T., McMeeking, G. R., Sullivan, A. P., et al. (2014). Characteristics of atmospheric ice nucleating particles associated with biomass burning in the US: Prescribed burns and wildfires. *Journal of Geophysical Research: Atmospheres*, *119*(17), 10458–10470. <https://doi.org/10.1002/2014JD021980>
- McNaughton, C. S., Clarke, A. D., Howell, S. G., Pinkerton, M., Anderson, B., Thornhill, L., et al. (2007). Results from the DC-8 inlet characterization experiment (DICE): Airborne vs. surface sampling of mineral dust and sea salt aerosols. *Aerosol Science and Technology*, *41*(2), 136–159. <https://doi.org/10.1080/02786820601118406>
- Misra, M. K., Ragland, K. W., & Baker, A. J. (1993). Wood ash composition as a function of furnace temperature. *Biomass and Bioenergy*, *4*(2), 103–116. [https://doi.org/10.1016/0961-9534\(93\)90032-Y](https://doi.org/10.1016/0961-9534(93)90032-Y)
- Molina, L. T., Madronich, S., Gaffney, J. S., Apel, E., de Foy, B., Fast, J., et al. (2010). An overview of the MILAGRO 2006 Campaign: Mexico City emissions and their transport and transformation. *Atmospheric Chemistry and Physics*, *10*(18), 8697–8760. <https://doi.org/10.5194/acp-10-8697-2010>
- Nault, B. A., Campuzano-Jost, P., Day, D. A., Schroder, J. C., Anderson, B., Beyersdorf, A. J., et al. (2018). Secondary organic aerosol production from local emissions dominates the organic aerosol budget over Seoul, South Korea, during KORUS-AQ. *Atmospheric Chemistry and Physics*, *18*(24), 17769–17800. <https://doi.org/10.5194/acp-18-17769-2018>
- Oberdörster, G., Oberdörster, E., & Oberdörster, J. (2005). Nanotoxicology: An emerging discipline evolving from studies of ultrafine particles. *Environmental Health Perspectives*, *113*(7), 823–839. <https://doi.org/10.1289/ehp.7339>
- Pardo, M., Li, C., He, Q., Levin-Zaidman, S., Tsoory, M., Yu, Q., et al. (2020). Mechanisms of lung toxicity induced by biomass burning aerosols. *Particle and Fibre Toxicology*, *17*(1), 4. <https://doi.org/10.1186/s12989-020-0337-x>
- Parks, S. A., Miller, C., Parisien, M.-A., Holsinger, L. M., Dobrowski, S. Z., & Abatzoglou, J. (2015). Wildland fire deficit and surplus in the western United States, 1984–2012. *Ecosphere*, *6*(12), 1–13. <https://doi.org/10.1890/ES15-00294.1>
- Permar, W., Wang, Q., Selimovic, V., Wielgasz, C., Yokelson, R. J., Hornbrook, R. S., et al. (2021). Emissions of trace organic gases from western US wildfires based on WECAN aircraft measurements. *Journal of Geophysical Research: Atmospheres*, *126*, e2020JD033838. <https://doi.org/10.1029/2020JD033838>
- Radke, L. F., Hegg, D. A., Hobbs, P. V., Nance, J. D., Lyons, J. H., Laursen, K. K., et al. (1991). Particulate and trace gas emissions from large biomass fire in North America. In J. S. Levine (Ed.), *Global biomass burning: Atmospheric, climatic, and biospheric implications* (pp. 209–216). The MIT Press.
- Raison, R. J., Khanna, P., & Woods, P. (1985). Transfer of elements to the atmosphere during low-intensity prescribed fires in three Australian subalpine eucalypt forests. *Canadian Journal of Forest Research*, *15*, 657–664. <https://doi.org/10.1139/x85-107>
- Reid, C. E., Brauer, M., Johnston, F. H., Jerrett, M., Balmes, J. R., & Elliott, C. T. (2016). Critical review of health impacts of wildfire smoke exposure. *Environmental Health Perspectives*, *124*(9), 1334–1343. <https://doi.org/10.1289/ehp.1409277>
- Reid, J. S., & Hobbs, P. V. (1998). Physical and optical properties of young smoke from individual biomass fires in Brazil. *Journal of Geophysical Research: Atmospheres*, *103*(D24), 32013–32030. <https://doi.org/10.1029/98jd00159>
- Reisen, F., Duran, S. M., Flannigan, M., Elliott, C., & Rideout, K. (2015). Wildfire smoke and public health risk. *International Journal of Wildland Fire*, *24*(8), 1029. <https://doi.org/10.1071/wf15034>
- Ruth, U., Barbante, C., Bigler, M., Delmonte, B., Fischer, H., Gabrielli, P., et al. (2008). Proxies and measurement techniques for mineral dust in Antarctic ice cores. *Environmental Science & Technology*, *42*(15), 5675–5681. <https://doi.org/10.1021/es703078z>
- Scheuer, E., Talbot, R. W., Dibb, J. E., Seid, G. K., DeBell, L., & Lefler, B. (2003). Seasonal distributions of fine aerosol sulfate in the North American Arctic basin during TOPSE. *Journal of Geophysical Research*, *108*(D4). <https://doi.org/10.1029/2001jd001364>
- Schill, G. P., Froyd, K. D., Bian, H., Kupc, A., Williamson, C., Brock, C. A., et al. (2020). Widespread biomass burning smoke throughout the remote troposphere. *Nature Geoscience*, *13*(6), 422–427. <https://doi.org/10.1038/s41561-020-0586-1>
- Schwarz, J. P., Gao, R. S., Spackman, J. R., Watts, L. A., Thomson, D. S., Fahey, D. W., et al. (2008). Measurement of the mixing state, mass, and optical size of individual black carbon particles in urban and biomass burning emissions. *Geophysical Research Letters*, *35*(13). <https://doi.org/10.1029/2008gl033968>

- Sedlacek, A. J., Buseck, P. R., Adachi, K., Onasch, T. B., Springston, S. R., & Kleinman, L. (2018). Formation and evolution of tar balls from northwestern US wildfires. *Atmospheric Chemistry and Physics*, 18(15), 11289–11301. <https://doi.org/10.5194/acp-18-11289-2018>
- Selimovic, V., Yokelson, R. J., McMeeking, G. R., & Coefield, S. (2020). Aerosol mass and optical properties, smoke influence on O<sub>3</sub>, and high NO<sub>3</sub> production rates in a western US city impacted by wildfires. *Journal of Geophysical Research: Atmospheres*, 125(16). <https://doi.org/10.1029/2020jd032791>
- Sparks, T. L., & Wagner, J. (2021). Composition of particulate matter during a wildfire smoke episode in an urban area. *Aerosol Science and Technology*, 55, 1–747. <https://doi.org/10.1080/02786826.2021.1895429>
- Tang, M., Cziczo, D. J., & Grassian, V. H. (2016). Interactions of water with mineral dust aerosol: Water adsorption, hygroscopicity, cloud condensation, and ice nucleation. *Chemical Reviews*, 116(7), 4205–4259. <https://doi.org/10.1021/acs.chemrev.5b00529>
- Umo, N. S., Murray, B. J., Baeza-Romero, M. T., Jones, J. M., Lea-Langton, A. R., Malkin, T. L., et al. (2015). Ice nucleation by combustion ash particles at conditions relevant to mixed-phase clouds. *Atmospheric Chemistry and Physics*, 15(9), 5195–5210. <https://doi.org/10.5194/acp-15-5195-2015>
- van der Werf, G. R., Randerson, J. T., Giglio, L., van Leeuwen, T. T., Chen, Y., Rogers, B. M., et al. (2017). Global fire emissions estimates during 1997–2016. *Earth System Science Data*, 9(2), 697–720. <https://doi.org/10.5194/essd-9-697-2017>
- Vassilev, S. V., Baxter, D., Andersen, L. K., & Vassileva, C. G. (2010). An overview of the chemical composition of biomass. *Fuel*, 89(5), 913–933. <https://doi.org/10.1016/j.fuel.2009.10.022>
- Vassilev, S. V., Baxter, D., Andersen, L. K., & Vassileva, C. G. (2013). An overview of the composition and application of biomass ash. Part 1. Phase-mineral and chemical composition and classification. *Fuel*, 105, 40–76. <https://doi.org/10.1016/j.fuel.2012.09.041>
- Vassilev, S. V., Baxter, D., Andersen, L. K., Vassileva, C. G., & Morgan, T. J. (2012). An overview of the organic and inorganic phase composition of biomass. *Fuel*, 94, 1–33. <https://doi.org/10.1016/j.fuel.2011.09.030>
- Wagner, J., Naik-Patel, K., Wall, S., & Harnly, M. (2012). Measurement of ambient particulate matter concentrations and particle types near agricultural burns using electron microscopy and passive samplers. *Atmospheric Environment*, 54, 260–271. <https://doi.org/10.1016/j.atmosenv.2012.01.067>
- Yokelson, R. J., Burling, I. R., Urbanski, S. P., Atlas, E. L., Adachi, K., Buseck, P. R., et al. (2011). Trace gas and particle emissions from open biomass burning in Mexico. *Atmospheric Chemistry and Physics*, 11(14), 6787–6808. <https://doi.org/10.5194/acp-11-6787-2011>
- Yokelson, R. J., Crounse, J. D., DeCarlo, P. F., Karl, T., Urbanski, S., & Atlas, E., et al. (2009). Emissions from biomass burning in the Yucatan. *Atmospheric Chemistry and Physics*, 9(15), 5785–5812. <https://doi.org/10.5194/acp-9-5785-2009>
- Zhang, J., Liu, L., Xu, L., Lin, Q., Zhao, H., Wang, Z., et al. (2020). Exploring wintertime regional haze in northeast China: Role of coal and biomass burning. *Atmospheric Chemistry and Physics*, 20(9), 5355–5372. <https://doi.org/10.5194/acp-20-5355-2020>

## References From the Supporting Information

- Adachi, K., Sedlacek, A. J., Kleinman, L., Chand, D., Hubbe, J. M., & Buseck, P. R. (2018). Volume changes upon heating of aerosol particles from biomass burning using transmission electron microscopy. *Aerosol Science and Technology*, 52(1), 46–56. <https://doi.org/10.1080/02786826.2017.1373181>
- Buseck, P. R., Adachi, K., Gelencsér, A., Tompa, É., & Pósfai, M. (2014). Ns-soot: A material-based term for strongly light-absorbing carbonaceous particles. *Aerosol Science and Technology*, 48(7), 777–788. <https://doi.org/10.1080/02786826.2014.919374>
- Cappa, C. D., Onasch, T. B., Massoli, P., Worsnop, D. R., Bates, T. S., Cross, E. S., et al. (2012). Radiative absorption enhancements due to the mixing state of atmospheric black carbon. *Science*, 337(6098), 1078–1081. <https://doi.org/10.1126/science.1223447>
- Engelbrecht, J. P., Moosmüller, H., Pincock, S., Jayanty, R. K. M., Lersch, T., & Casuccio, G. (2016). Technical note: Mineralogical, chemical, morphological, and optical interrelationships of mineral dust re-suspensions. *Atmospheric Chemistry and Physics*, 16(17), 10809–10830. <https://doi.org/10.5194/acp-16-10809-2016>
- Hu, W., Campuzano-Jost, P., Day, D. A., Croteau, P., Canagaratna, M. R., Jayne, J. T., et al. (2017). Evaluation of the new capture vaporizer for aerosol mass spectrometers (AMS) through field studies of inorganic species. *Aerosol Science and Technology*, 51(6), 735–754. <https://doi.org/10.1080/02786826.2017.1296104>
- Jimenez, J. L. (2003). Ambient aerosol sampling using the Aerodyne aerosol mass spectrometer. *Journal of Geophysical Research*, 108(D7). <https://doi.org/10.1029/2001jd001213>
- Kleinman, L. I., Sedlacek, A. J., Adachi, K., Buseck, P. R., Collier, S., Dubey, M. K., et al. (2020). Rapid evolution of aerosol particles and their optical properties downwind of wildfires in the western US. *Atmospheric Chemistry and Physics*, 20(21), 13319–13341. <https://doi.org/10.5194/acp-20-13319-2020>
- Lai, A. M., Shafer, M. M., Dibb, J. E., Polashenski, C. M., & Schauer, J. J. (2017). Elements and inorganic ions as source tracers in recent Greenland snow. *Atmospheric Environment*, 164, 205–215. <https://doi.org/10.1016/j.atmosenv.2017.05.048>
- Yokelson, R. J., Crounse, J. D., DeCarlo, P. F., Karl, T., Urbanski, S., Atlas, E., et al. (2009). Emissions from biomass burning in the Yucatan. *Atmospheric Chemistry and Physics*, 9(15), 5785–5812. <https://doi.org/10.5194/acp-9-5785-2009>